

Department of Physics, Chemistry and Biology

Master's Thesis

Search for Dark Matter in the Upgraded High Luminosity LHC at CERN

Impact of ATLAS phase II performance on a mono-jet analysis

Sven-Patrik Hallsjö

Thesis work performed at Stockholm University

Linköping, June 4, 2014

LITH-IFM-A-EX--14/2863--SE



**Linköpings universitet
TEKNISKA HÖGSKOLAN**

Department of Physics, Chemistry and Biology
Linköping University
SE-581 83 Linköping, Sweden

Search for Dark Matter in the Upgraded High Luminosity LHC at CERN

Impact of ATLAS phase II performance on a mono-jet analysis

Sven-Patrik Hallsjö

Thesis work performed at Stockholm University

Linköping, June 4, 2014

Supervisor: **Docent Christophe Clément**
 FYSIKUM Stockholm University
Professor Magnus Johansson
 IFM, Linköping University

Examiner: **Professor Magnus Johansson**
 IFM, Linköping University



Avdelning, Institution
Division, Department

Theoretical physics group
Department of Physics, Chemistry and Biology
SE-581 83 Linköping

Datum
Date

2014-06-04

Språk
Language

Svenska/Swedish
 Engelska/English

Rapporttyp
Report category

Licentiatavhandling
 Examensarbete
 C-uppsats
 D-uppsats
 Övrig rapport

ISBN
—

ISRN
LITH-IFM-A-EX--14/2863--SE

Serietitel och serienummer **ISSN**
Title of series, numbering —

URL för elektronisk version

<http://urn.kb.se/resolve?urn=urn:nbn:se:liu:diva-XXXXXX>

Titel Sökandet efter mörk materia i den uppgraderade hög luminositets LHC i CERN
Title Search for Dark Matter in the Upgraded High Luminosity LHC at CERN

Undertitel Påverkan av ATLAS fas II prestanda på en mono-jet analys
Subtitle Impact of ATLAS phase II performance on a mono-jet analysis

Författare Sven-Patrik Hallsjö
Author

Sammanfattning
Abstract

Disclaimer: Abstract not yet completed.

Something as an introduction:

The LHC at CERN is undergoing an upgrade to increase the center of mass energy for the colliding particles which means that new physical processes will be explored. One drawback of this is that it will be harder to isolate unique particle collisions since more and more collisions will occur simultaneously, so called pile-up.

One hope for the upgrade is that WIMP models of dark matter will be detected.

This thesis covers looking at effective operators which try to explain dark matter without adding new theories to the standard model or QFT.

Some results and a slight conclusion.

Nyckelord

Keywords

Disclaimer: This not yet completed., ATLAS, Beyond standard model physics, CERN, Dark matter, Elementary particle physics, High energy physics, something, this is in mythesis.sty

4 **Abstract**

5 **Disclaimer: Abstract not yet completed.**

6 Something as an introduction:

7 The LHC at CERN is undergoing an upgrade to increase the center of mass en-
8 ergy for the colliding particles which means that new physical processes will be
9 explored. One drawback of this is that it will be harder to isolate unique parti-
10 cle collisions since more and more collisions will occur simultaneously, so called
11 pile-up.

12 One hope for the upgrade is that WIMP models of dark matter will be detected.

13 This thesis covers looking at effective operators which try to explain dark matter
14 without adding new theories to the standard model or QFT.

15 Some results and a slight conclusion.

16 **Acknowledgments**

17 [REDACTED]

18 A big thank you to my family, fiancée and friends who have supported me through-
19 out my education. A warm thank you to my friend Joakim Skoog who altered
20 some of the images for me.

21 [REDACTED]

22 [REDACTED]

23 *Linköping, June 2014*
24 *Sven-Patrik Hallsjö*

Contents

Notation

1 Introduction

1.1	Research goals	2
1.2	Theoretical Background	3
1.2.1	Quantum mechanics and quantum field theory	3
1.2.2	Nuclear, particle and subatomic particle physics	4
1.2.3	The standard model of particle physics	4
1.2.4	Dark matter	5
1.2.5	Effective field theory	6
1.2.6	Search for WIMPS	8
1.3	Experimental overview	10
1.3.1	LHC	10
1.3.2	ATLAS	11
1.3.3	Coordinate system	12
1.3.4	Reconstructing data	12
1.3.5	Pile-up	13
1.3.6	Mono-jet analysis	13
1.3.7	Phase II high luminosity upgrade	14
1.3.8	Monte Carlo simulation	15

2 Validation of smearing functions

2.1	Smearing functions	18
2.1.1	Electron and photon	18
2.1.2	Muon	18
2.1.3	Tau	18
2.1.4	Jets	18
2.1.5	Missing Transversal Energy	18
2.2	Validation	20
2.2.1	Method	20
2.3	Results	21
2.3.1	Electron and photon	22
2.3.2	Muon	23

58	2.3.3 Tau	23
59	2.3.4 Jets	24
60	2.3.5 Missing Transversal Energy	25
61	2.4 Expected results	26
62	2.5 Discussion	28
63	2.5.1 Smearing independent on pile-up	28
64	2.5.2 Comparison to expected results	28
65	2.6 Conclusion	29
66	3 Evaluating dark matter signals	31
67	3.1 Signal to background ratio	32
68	3.1.1 Signal Region	32
69	3.1.2 Weight	32
70	3.1.3 Verification of background normalization	32
71	3.1.4 Errors in data	33
72	3.1.5 Figure of merit	33
73	3.1.6 D5 operator models	35
74	3.1.7 Light vector mediator models	35
75	3.2 Signal region definitions	36
76	3.2.1 Signal regions	36
77	3.2.2 Verifying background data	36
78	3.3 Mitigating the effect of the high luminosity	36
79	3.4 Results	37
80	3.4.1 Verifying background data	37
81	3.4.2 Events	37
82	3.4.3 Limit on M^*	39
83	3.4.4 Limit on mediator mass	41
84	3.5 Discussion	43
85	3.5.1 Comparison to previous results	43
86	3.5.2 Effect of the high luminosity	43
87	3.6 Conclusion	45
88	3.6.1 Limit on M^*	45
89	3.6.2 Limit on mediator mass	45
90	3.6.3 Effect of the high luminosity	45
91	4 Results and Conclusions	47
92	4.1 Validation of smearing functions	47
93	4.2 Signal to background ratio	48
94	4.2.1 Limit on M^*	48
95	4.2.2 Limit on mediator mass	48
96	4.3 Other selection criteria and observables	48
97	4.3.1 Limit on M^*	48
98	4.3.2 Limit on mediator mass	48
99	4.4 Mitigating the effect of the high luminosity	48
100	4.5 Recommendations to mitigate the effect of the high luminosity	48
101	4.6 Suggestions for future research	48

102	A Datasets	51
103	A.1 Background processes	51
104	A.1.1 Validation	51
105	A.1.2 Background to signals	51
106	A.2 Signals	52
107	A.2.1 Qcut	52
108	A.2.2 D5 signal processes	52
109	A.2.3 Light vector mediator processes	52
110	Bibliography	55

Notation

NOTATIONS

Notation	Explanation
barn(b)	$1 \text{ barn}(b) = 10^{-24} \text{ cm}^2$
\oplus	$a \oplus b = \sqrt{a^2 + b^2}$, $a \oplus b \oplus c = \sqrt{a^2 + b^2 + c^2}$

ABBREVIATIONS

Abbreviation	Expansion
ATLAS	A large Toroidal LHC ApparatuS
CERN	Organisation européenne pour la recherche nucléaire ¹
CMS	Compact Muon Solenoid
CR	Control Region
LHC	Large Hadron Collider
MC	Monte Carlo
RMS	Root Mean Square
SM	the Standard Model of particle physics
SR	Signal Region
WIMP	Weakly Interacting Massive Particle
WIMPS	Weakly Interacting Massive ParticleS
QED	Quantum ElectroDynamics
QFT	Quantum Field Theory
QM	Quantum Mechanics

¹Originally, Conseil Européen pour la Recherche Nucléaire

1

Introduction

117 Discrepancies in measurements of the rotations of galaxies indicate the presence
118 of a large amount of matter which interacts through gravity, though not elec-
119 tromagnetically making it invisible to our telescopes. This matter is commonly
120 referred to as dark matter. Since no known or hypothesised particle in the stan-
121 dard model of particle physics can be used as a candidate for dark matter, this
122 hints at the presence of new physics.

123 At the Organisation Européene pour la Recherche Nucléaire (CERN) focus now
124 lies to discover any evidence of so called weakly interacting massive particles
125 (WIMPS) which may be a candidate for dark matter. It is usually impossible to
126 detect any interaction of dark matter candidates on the subatomic scale, however
127 through looking at proposed interactions, searching for assumed decay channels
128 and by investigating what is invisible to the detectors by using momentum con-
129 servation it is hoped that signs will be found. Though to date, none have been
130 found.

131 Both experiments and current theories now show that higher energies are re-
132 quired at the LHC to be able to see any signs. This is why the LHC and all detectors
133 are undergoing a vast upgrade program [1]. In this thesis focus will be on the last
134 part of the upgrade due for completion in 2023, known as the high luminosity-
135 LHC phase II upgrade; and also on the ATLAS detector. The method used in this
136 thesis focuses on looking at data which emulate conditions at the upgraded LHC.

137 1.1 Research goals

138 This research took place at Stockholm University from January 7th until **when**?
139 During the research period the following tasks were set up and performed/answered:

- 140 • Implement a C++ programme that loops over the collisions inside the signal
141 and background datasets.
- 142 • For each collision retrieve the relevant observables (variables used to extract
143 the signal over the background) and apply "smearing functions" to emulate
144 the effect of the high luminosity on the observables.
- 145 • For both signal and background datasets, compare observables before and
146 after smearing. What observables are the least/most affected?
- 147 • Implement selection criteria that selects the signal collisions efficiently while
148 reduces significantly the background. In a first step the selection criteria
149 should be taken from existing studies.
- 150 • Selection criteria can be evaluated and compared with each other using a
151 figure of merit P , that measures the sensitivity of the experiment to the dark
152 matter signal. Calculate P for the given selection criteria before and after
153 smearing.
- 154 • What is the effect of the high luminosity (smearing) on the value of P ?
- 155 • Investigate other selection criteria and observables, to mitigate the effect of
156 high luminosity. Use P to rank different criteria after smearing.
- 157 • Conclude on the effect of the high luminosity on the sensitivity for dark matter
158 and possible ways to mitigate its effects using alternative observables
159 and selection criteria.

1.2 Theoretical Background

1.2.1 Quantum mechanics and quantum field theory

In the beginning of the 20th century, some physical phenomena could not be explained by classical physics, for example the ultra-violet disaster of any classical model of black-body radiation, and the photoelectric effect [2]. It was these phenomena that led to the formulation of quantum mechanics (QM), where energy transfer is quantized and particles can act as both waves and particles at the same time [3].

Combining QM with classical electromagnetism proved harder than expected, colliding a photon(em-field) and an electron (particle/wave) is quite tricky. This can be seen when trying to calculate the scattering between them both in a QM schema. One idea that came from this was to explain them both in the same framework, field theory. Also, trying to incorporate special relativity into QM suggested a field description where space-time is described using the metric formalism from differential geometry. The culmination of both of these problems is the first part of a Quantum field theory (QFT), Quantum electrodynamics (QED) which with incredible precision explains electromagnetic phenomena including effects from special relativity[4]. It is in this merging that antimatter was theorised, since it is a requirement for the theory to hold. After the discovery of antimatter, the theory was set in stone. Since this the theory has been altered somewhat to explain more and more experimental data. This is discussed more in subsection 1.2.2 and subsection 1.2.3.

To be able to calculate properties in QFT one uses the Lagrangian formalism [5], which gives a governing equation for the different physical processes. In general the Lagrangian used for the Standard model is quite complicated, one can thus focus on one of the different terms corresponding to a specific interaction. This can be done to calculate the so called cross-section for a process, which is related to the probability that that process will occur. A step to simplify the calculations is to use the so called Feynman diagrams, an example of which is given in figure 1.1.

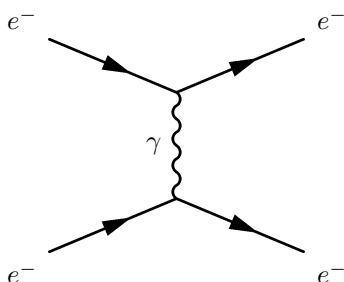


Figure 1.1: An example of a Feynman diagram explaining an electron-electron scattering using QED.

Through the figure, which comes with certain rules, and knowing what the major process (in this case QED) one can calculate the cross-section [4]. It is this that is needed to predict what one will be able to detect new particles.

1.2.2 Nuclear, particle and subatomic particle physics

Many could argue that these branches of physics started after Ernest Rutherford famous gold foil experiment [6], where he discovered that matter is composed of matter with a nucleus, a lot of empty space and electrons.

It was this that sparked the curiosity to see what the nucleus is made of and what forces govern the insides of atoms. After this, and the combination of the theoretical description given by QM, a lot more has been discovered and still more has been predicted. The newest of these is of course the Higgs particle, which was predicted through QFT and then discovered by the ATLAS and the CMS experiments at CERN [7].

The discovered particles are often divided into different groups depending on the fundamental particles that build them up. For instance, particles build up of three quarks are known as hadrons. Particles with an integer spin are known as bosons whereas half-integer particles are known as fermions.

1.2.3 The standard model of particle physics

The standard model of particle physics, referred to simply as the standard model (SM), is the particle zoo which tries to categorize all the particles and that have been discovered experimentally. QFT explains the interactions between these particles and it has also predicted several particles by including symmetries [6]. Regarding SM, Gauge bosons are the force carriers for the different forces, quarks are the and leptons are the fundamental blocks that we know of so far. The difference between the later two is if they interact via the strong force or not.

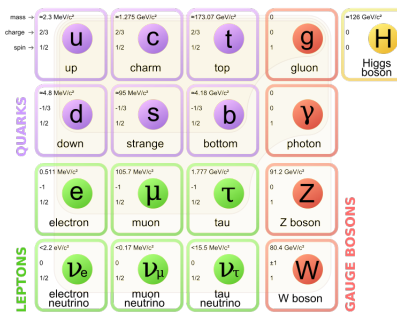


Figure 1.2: The standard model of particle physics where the three first columns represent the so called generations, starting with the first. [8].

SM is today the pinnacle of particle physics and can be used to explain almost everything that occurs around us. There are however some problems [9]:

- There is no link between gravity and the SM.
- Asymmetry between matter and antimatter can not be fully explained.
- No dark matter candidate!
- No explanation that can contain dark matter.

221 In this thesis focus lies with dark matter, some more introduction to possible
 222 dark matter and different candidates in extensions to SM are explained in subsection
 223 1.2.4.

224 1.2.4 Dark matter

225 Dark matter is among other things, the name given to the solution to the discrepancies
 226 of galactic rotations.

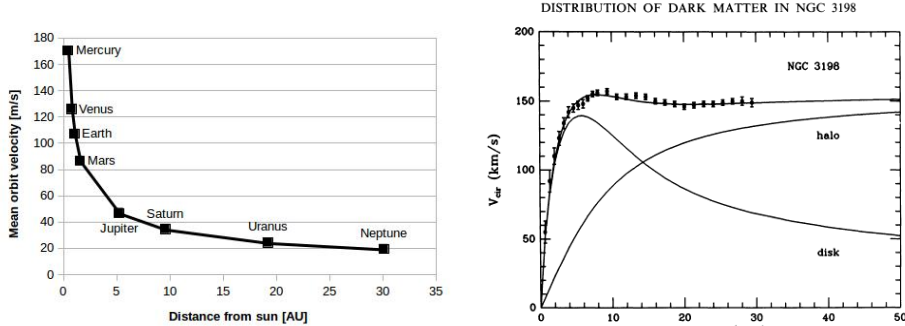
227 To explain this, focus on matter in a galaxy which are rotating around the center
 228 of the galaxy. Through Newtons law of gravity and the centrifugal force one can
 229 calculate the rotation speed dependent on the distance to the center of the galaxy.
 230 Since one of these forces is attractive and the other repulsive, if the matter is in
 231 a stable orbit around the galactic center (which they are) they must be equal and
 232 give us an expression for the speed depending on the distance. Newtons law can
 233 be written as the following:

$$F_{Gravitational} = G \frac{Mm}{r^2} = G_M \frac{m}{r^2} \quad F_{Centrifugal} = m \frac{V^2}{r} \quad (1.1)$$

234 where G is the gravitational constant, M the mass of the centre object, m the mass
 235 of the matter, r the distance between the two and V is the rotation speed. It has
 236 been simplified using G_M since all matter orbits the same galactic center. Setting
 237 the equations in (1.1) results in:

$$G_M \frac{m}{r^2} = m \frac{V^2}{r} \Leftrightarrow V^2 = \frac{G_M}{r} \Rightarrow V = \sqrt{\frac{G_M}{r}} \propto \frac{1}{\sqrt{r}} \quad (1.2)$$

238 where the speed is assumed to be positive and \propto means proportional. Through
 239 these simple calculations it shown that the rotation speed should decrease with
 240 and increased distance. The same reasoning can be applied to our solar system
 241 where this is the case figure 1.3a. The relation in these units is $V = \frac{107}{\sqrt{r}}$ where
 242 107 can be used in (1.2) to calculate the mass of the sun. However when looking
 243 at galaxies, even when taking into account that one has to see the galaxies as a
 244 mass distribution and that the above is only true when outside of the inner mass
 245 half, this is not the case! In figure 1.3b experimental data can be seen from the
 246 galaxy NGC3198 with a fitted curve which does not decrease with the distance
 247 but is instead constant. This is the discrepancy which is solved by postulating
 248 the existence of dark matter. After this the big question arises, what could this
 249 dark matter consist of? What is known so far lies in the name. It is called dark
 250 since there is no electromagnetic interaction and matter since it has gravitational
 251 interaction. This means that it can not be made up of any baryonic matter or
 252 anything in the Standard Model apart from neutrinos. The main interest of this
 253 thesis and also the main contributor to the rotational discrepancies is known as
 254 cold dark matter. This is due to the matter having a low speed, thus low kinetic
 255 energy, and have a high particle mass (In the GeV scale) [9, 12, 13]. This means
 256 however that neutrinos can not be a candidate, thus dark matter can not be made
 257 out of any standard model particles. There are several ideas to detected dark
 258 matter, [9]



(a) Rotation speed of planets in our solar system. Since the distance is quite small on an astronomical scale, there is no sign of dark matter. Based on data from [10].

(b) Rotation speed of matter in NGC3198 with a curve fitting and three different models, if only a dark model halo existed, if there was no dark matter and the correct, if both exist [11].

Figure 1.3: Different rotation curves, both for planets in our solar system and matter in the NGC3198 galaxy.

- Ordinary matter interacting with ordinary matter can produce dark matter, known as production. Which is the processes that occurs at particle accelerators.
- Dark matter interacting with ordinary matter can produce dark matter, known as direct detection.
- Dark matter interacting with dark matter can produce ordinary matter, known as indirect detection.

In this thesis the focus lies with production. There are several theories how to detect dark matter in proton-proton collisions such that occur at the LHC at CERN this is covered more in subsection 1.2.6.

1.2.5 Effective field theory

In quantum field theory the objective is usually to find the part of the Lagrangian which explains a type of interaction, known as the operator of the interaction and also to find the probability amplitude (cross-section) for a certain interaction. For complicated processes it is easier to employ certain conditions so that the small scale phenomena are simplified and the whole picture understood. This is known as using an effective field theory and the concept is explained in figure 1.4. The operator can be found through assuming the possible interactions and using the effective field theory [4]. The cross-sections can be found through the Feynman diagrams as described in subsection 1.2.1.

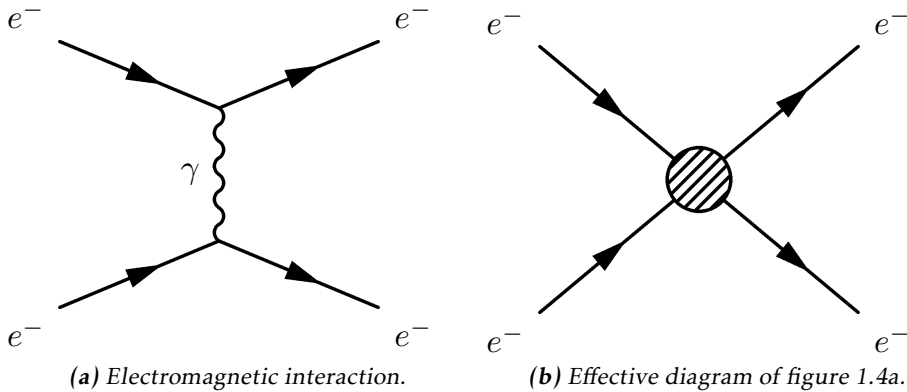


Figure 1.4: Feynman diagram of an electron-electron scattering, both as an ordinary diagram and as its effective theory version, where the details are hidden in the blob.

In this thesis the same effective field theory as in Refs. [12, 14] will be considered. The WIMP (usually denoted χ) is assumed to be the only particle in addition to the standard model fields. It is assumed that an even number of χ must be in every coupling. It is assumed that the mediator exists is heavier than the WIMPS, meaning that their interactions are in higher order terms of the effective field theory and thus not included in the operators. For simplicity, the WIMPS are assumed to be SM singlets, thus invariant under SM gauge transformations, and the coupling to the Higgs boson is neglected.

The operators used in this thesis are assumed to be quark bilinear operators on the form $\bar{q}\Gamma q$ where Γ is a 4×4 matrix of the complete set,

$$\Gamma = \{1, \gamma^5, \gamma^\mu, \gamma^\mu \gamma^5, \sigma^{\mu\nu}\} \quad (1.3)$$

This will dictate how the operators are written, more of why this is done can be found in [4, 12, 14].

This defines an effective field theory of the interaction of singlet WIMPs with hadronic matter. It is an approximation which will break down when the mediator mass is close to the mass of the WIMP. The condition for this is derived in [14] and gives:

$$M > 2m_\chi \quad (1.4)$$

where m_χ is the mass of the WIMP and M is the mass of the mediator particle. There is also the requirement that:

$$M \lesssim 4\pi M_* \quad (1.5)$$

where M_* is the energy scale where the effective theory is no longer a good approximation.

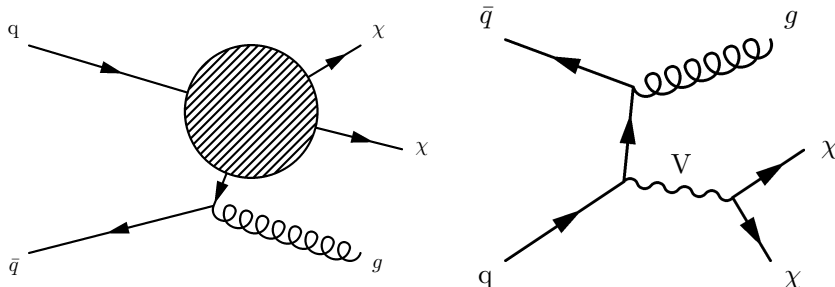
²⁹⁹ In this work, WIMPS are assumed to be Dirac fermions (half integer spin and is
³⁰⁰ not its own antiparticle).

³⁰¹ In table 1.1 the operators which are integrated out via the effective field theory
³⁰² and are of interest in this thesis are given.

Name	Initial state	Type	Operator
D1	qq	scalar	$\frac{m_q}{M_*^3} \bar{\chi} \chi \bar{q} q$
D5	qq	vector	$\frac{1}{M_*^2} \bar{\chi} \gamma^\mu \chi \bar{q} \gamma_\mu q$
D8	qq	axial-vector	$\frac{1}{M_*^2} \bar{\chi} \gamma^\mu \gamma^5 \chi \bar{q} \gamma_\mu \gamma^5 q$
D9	qq	tensor	$\frac{1}{M_*^2} \bar{\chi} \sigma^{\mu\nu} \chi \bar{q} \sigma_{\mu\nu} q$
D11	gg	scalar	$\frac{1}{4M_*^3} \bar{\chi} \chi \alpha_s (G_{\mu\nu}^a)^2$

Table 1.1: Table based on discussion in [13].

³⁰³ Where D denotes that the WIMPS are assumed to be Dirac fermions. These can all
³⁰⁴ be described using figure 1.5a.



(a) Effective Feynman diagram explaining the D-operators. **(b)** Feynman diagram describing the vector mediator model.

Figure 1.5: Feynman diagrams describing the signal models used in this thesis.

³⁰⁵ Another model which is considered is a vector mediator model which is described
³⁰⁶ by figure 1.5b.

1.2.6 Search for WIMPS

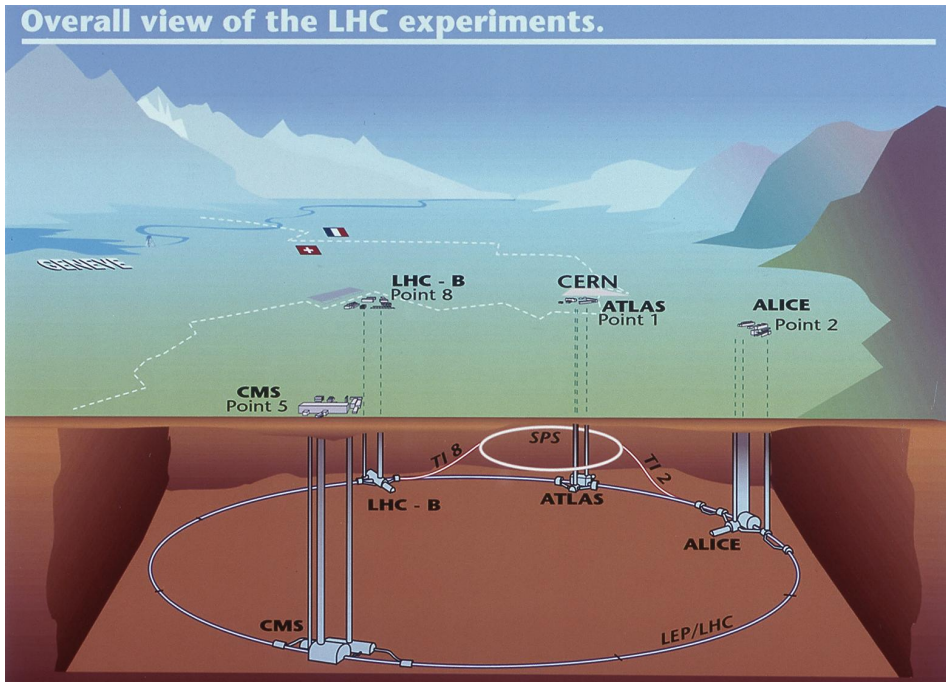
³⁰⁸ The search for WIMPS is based on a mono-jet analysis which is described in sub-
³⁰⁹ section 1.3.6. This method revolves around a high energetic jet which arises from
³¹⁰ the gluon from figure 1.5b and momentum missing from the energy conservation.

- 311 This means that something has happened which the detectors can not detect. If
312 the models from subsection 1.2.5 can explain the missing energy, then a model
313 for WIMPS has been found.
- 314 Since the search for WIMPS at the LHC is based on looking at the missing energy,
315 not actual detection, the experiment can not establish if a WIMP is stable on a
316 cosmological time scale and thus if it is a dark matter candidate [13]. This means
317 that if a candidate is found, it may still not be the dark matter that is needed to
318 explain the cosmological observations.
- 319 The different theories discussed in subsection 1.2.5 require some process in which
320 quarks and anti-quarks are produced. At ATLAS they have looked at proton-
321 proton collisions, in which they are produced, with 8 TeV center of mass energy
322 with out finding any excess of mono-jet events. This is why it is very interesting
323 that the LHC is undergoing a upgrade that will allow higher energy levels, see
324 subsection 1.3.7. With this the processes can be given higher energy and thus the
325 produced particles can be comprised of higher mass.

326 1.3 Experimental overview

327 1.3.1 LHC

328 The large hadron collider (LHC) is a particle accelerator located at CERN near
 329 Geneva in Switzerland, see figure 1.6. The accelerator was built to explore physics
 330 beyond the standard model and to make more accurate measurements of stan-
 331 dard model physics. Before it was shut down for an upgrade in 2012 it was able
 332 to accelerate two proton beams to such a velocity that each proton in them had
 333 an energy of 4 TeV which gives a center of mass energy, $\sqrt{s} = 8$ TeV. The proton
 334 beam is comprised of bunches of protons with enough spacing that bunch col-
 335 lisions can happen independent of each other. Apart from the energy, the rate at
 336 which the accelerator produces a certain process can be calculated through the
 337 instantaneous luminosity. For the LHC the instantaneous luminosity was 10^{34}
 338 $\text{cm}^{-2}\text{s}^{-1}$ [15] or $10\text{nb}^{-1}\text{s}^{-1}$ where $1 \text{ barn(b)} = 10^{-24} \text{ cm}^2$.



339 **Figure 1.6:** Figure showing the LHC and the different detector sites[16].

340 The instantaneous luminosity, often just denoted luminosity, can be defined in
 341 different ways depending on how the collision takes place. For two collinear
 intersecting particle beams it is defined as:

$$342 \mathcal{L} = \frac{f k N_1 N_2}{4\pi \sigma_x \sigma_y} \quad (1.6)$$

342 where N_i are the number of protons in each of the bunches, f is the frequency
 343 at which the bunches collide , k the number of colliding bunches in each beam,
 344 and σ_x (σ_y) is the horizontal (vertical) beam size at the interaction point. Since
 345 the instantaneous luminosity increases quadratically with more protons in each
 346 bunch, increasing the number of protons would be a good strategy to increase
 347 the instantaneous luminosity. However aside from the difficulties to create and
 348 maintain a beam with more particles, a large N_i increases the probability for
 349 multiple collisions per bunch crossing, referred to as pile-up. Pile up will be a
 350 key aspect which is described more in subsection 1.3.5.

351 The expected number of events can be calculated by using the instantaneous lu-
 352 minosity through the following:

$$N = \sigma \int \mathcal{L} dt \equiv \sigma \mathcal{L} \quad (1.7)$$

353 where \mathcal{L} is the integrated luminosity and σ is the cross section which is often
 354 measured in barn. The integrated luminosity is a measurement of total number
 355 of interactions that have occurred over time. Before the LHC was shut down \mathcal{L}
 356 was 20.8 fb^{-1} .

357 The cross section, as explained in subsection 1.2.1, is a measure of the effective
 358 surface area seen by the impinging particles, and as such is expressed in units
 359 of area. The cross section is proportional to the probability that an interaction
 360 will occur. It also provides a measure of the strength of the interaction between
 361 the scattered particle and the scattering center. Further details can be found in
 362 reference [17].

363 1.3.2 ATLAS

364 As seen in figure 1.6, there are several detectors at the LHC. One of these is
 365 ATLAS which is a general purpose detector that uses a toroid magnet. Its goal
 366 is to observe several different production and decay channels. The detector is
 367 composed of three concentric sub-detectors, the Inner detector, the Calorimeters
 368 and the Muon spectrometer [18].

369 The Inner detectors main task is to detect the tracks of the particles. It also mea-
 370 sures the position of the initial proton-proton collision.

371 The Calorimeters, electromagnetic and hadronic, are used to calculate the energy
 372 contained in the different particles. The electromagnetic detects particles which
 373 are charged, and the hadronic those which are neutral.

374 The Muon spectrometer is used to detect signs of muons, which will simply pass
 375 through the other detectors without leaving a trace. It also calculates the energy
 376 and momentum of the muons.

377 The neutrinos escape the ATLAS experiment without being detected, and in this
 378 thesis it is assumed that WIMPS pass through all the detectors without leaving
 379 any trace.

380 1.3.3 Coordinate system

381 The coordinate system of ATLAS, seen in figure 1.7 is a right-handed coordinate
 382 system with the x-axis pointing towards the centre of the LHC ring, and the z-axis
 383 along the tunnel/beam (counter clockwise) seen from above. The y-axis points up-
 384 ward. The origin is defined as the geometric center of the detector. A cylindrical
 385 coordinate system is also used for the transversal plane, (R, ϕ, Z) . For simplicity
 386 the pseudorapidity of particles from the primary vertex is defined as:

$$\eta = -\ln(\tan \frac{\theta}{2}) \quad (1.8)$$

387 where θ is the polar angle (xz-plane) of the particle direction measured from
 388 the positive z-axis. η is through this definition invariant under boosts in the z-
 389 direction.

390 It is quite common to calculate the distance between particles and jets in the
 391 (η, ϕ) space, $d = \sqrt{(\Delta\eta)^2 + (\Delta\phi)^2}$.

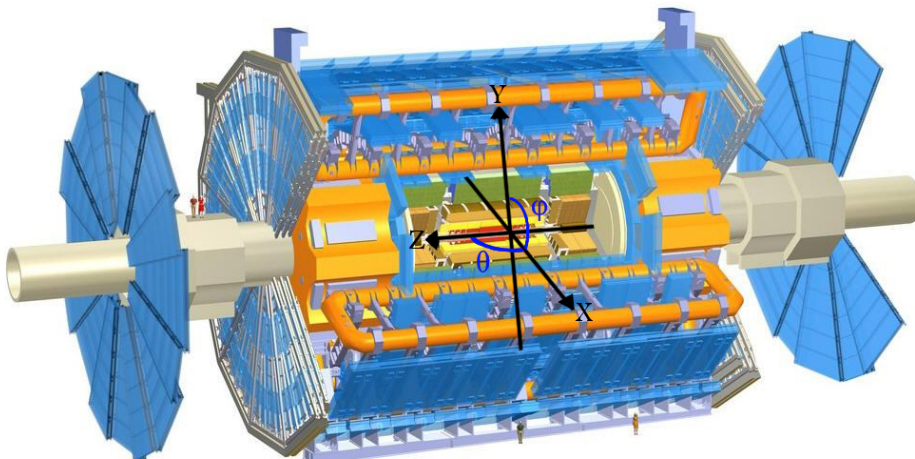


Figure 1.7: The ATLAS detector and the definition of the orthogonal Cartesian coordinate system. Image altered from[19]

392 1.3.4 Reconstructing data

393 To be able to compare the simulated data to real data it is important to include
 394 effects of the detectors. This is done using so called smearing functions which try
 395 to emulate the reconstruction of data.

396 The reconstruction process of data [18] is based on what response is given from
 397 the detectors. It is affected by pile-up and the energy of that which is detected.
 398 This process is not specifically used in the thesis, however the smearing functions
 399 are discussed in section 2.1.

400 1.3.5 Pile-up

401 Pile-up is the phenomena that several proton-proton collisions occur simultaneously.
 402 The number of pile-up is defined as the average number of proton-proton
 403 collisions that occur per bunch crossing per second. It is denoted as $\langle \mu \rangle$. μ can
 404 be calculated by adjusting a Poisson distribution to fit the curve created by the
 405 number of interactions per bunch crossing at a given luminosity. When this is
 406 done μ will be the mean value of the Poisson distribution.

407 1.3.6 Mono-jet analysis

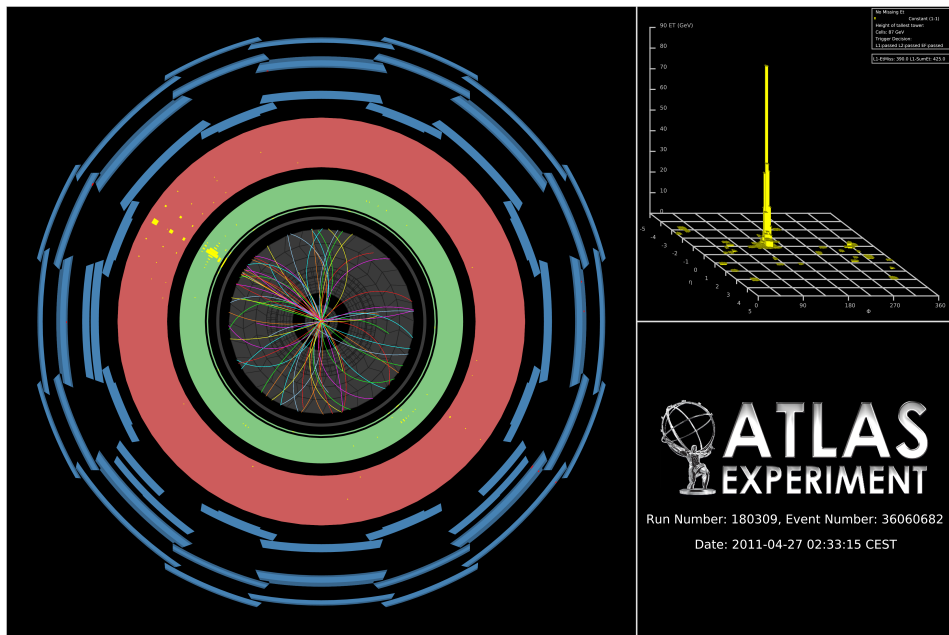


Figure 1.8: Image of an actual mono-jet event recorded by the ATLAS experiment [20].

408 When measuring the transversal energy one can in some interactions find incon-
 409 sistencies, such as jets that are in excess in one direction. In figure 1.8 one can see
 410 a high energetic jet which gives an excess of transversal energy in one direction
 411 after the collision. Since there is no balancing jet there must be transverse energy
 412 that is not detected, denoted E_T^{Miss} , since it was close to zero before the collision.
 413 This gives an indication that there energy to balance this that simply can not be
 414 detected. This could for instance be neutrinos or the sign of a new particle.

415 E_T^{Miss} is the modulus of the E_T^{Miss} vector which is defined as:

$$E_T^{\vec{M}iss} = -\sum E_T^{\vec{jet}} - \sum E_T^{\vec{Electron}} - \sum E_T^{\vec{\mu}on} - \sum E_T^{\vec{T}au} - \sum E_T^{\vec{\gamma}on} \quad (1.9)$$

416 Jets are hadrons which travel in the same direction and are usually created from

hadronization of a quark or a gluon in a collision. Usually jets are composed of a lot of energetic hadrons.

Since the jets are created from quarks or gluons, measuring a jet results in more information about the collision.

There are two main classes of events, signal and background. The signal corresponds to events that would arise from one of the processes in subsection 1.2.5. However to know that the missing energy is sign of the signal then one must understand all the other components that could contribute to the missing energy. Also there must be an excess of missing energy from what is expected from the background.

The background comprises of standard model processes that can mimic the mono-jet signature.

1.3.7 Phase II high luminosity upgrade

At the moment, the whole LHC is undergoing a step by step upgrade program which will be finalized around 2022-2023, denoted the high luminosity upgrade, or HL-upgrade. The upgrade consists of different stages, meaning that the upgrade will halt for periods so that experiments can take place. In figure 1.9 one can see

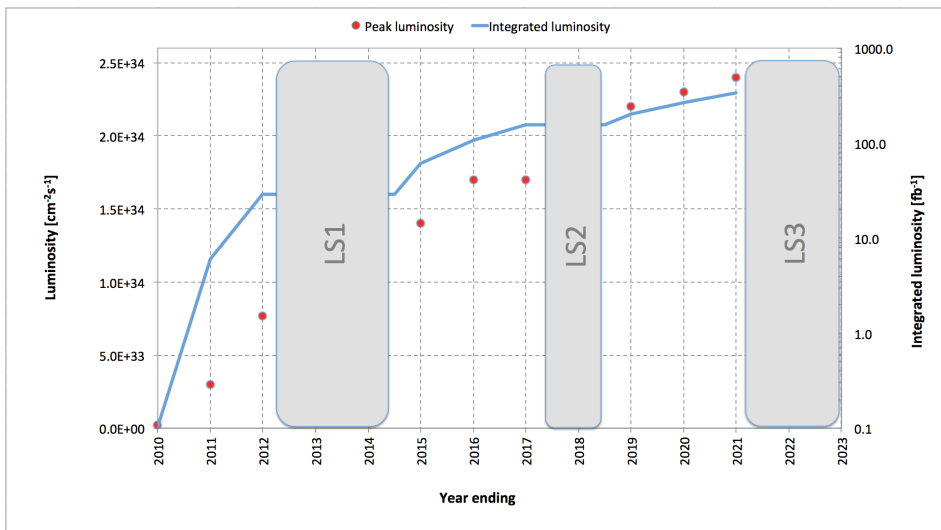


Figure 1.9: A graph showing the upgrading timetable with the instantaneous luminosity, denoted luminosity, and integrated luminosity expected in the different stages.

the three proposed upgrades. The period before LS1 is denoted phase 0, after LS1 and before LS2 phase I and after LS3 phase II.

LS1 is the upgrade which will take the LHC to its designed performance.

- 437 LS2 will take the LHC to the ultimate designed instantaneous luminosity.
 438 LS3 which is the focus of this thesis, will increase the instantaneous luminosity
 439 even more. Though for this to happen a modification of the whole LHC
 440 must be done, instead of just an upgrade and maintenance as before.

441 The following is expected for the experiments done after phase II:

Entity	Expected	Last run (2012)
Instantaneous luminosity	$\mathcal{L} \sim 50 \text{ nb}^{-1} \text{s}^{-1}$	$\mathcal{L} \sim 10 \text{ nb}^{-1} \text{s}^{-1}$
Integrated luminosity	$\mathcal{L} = 1000 - 3000 \text{ fb}^{-1}$	$\mathcal{L} = 20 \text{ fb}^{-1}$
Pile-up	$\langle \mu \rangle = 140$	$\langle \mu \rangle = 20$
Center of mass energy	$\sqrt{s} = 14 \text{ TeV}$	$\sqrt{s} = 8 \text{ TeV}$

Table 1.2: Expected running values for the Phase II HL-upgraded LHC with older values for comparison [21].

- 442 Where it should be noted that the integrated luminosity indicates the total amount
 443 of data which will be collected after the upgrade is completed before the next up-
 444 grade takes place.

445 1.3.8 Monte Carlo simulation

- 446 As mentioned before, in this thesis only emulated data has been used. This data
 447 is created by using a Monte Carlo (MC) simulation of the background processes
 448 and the expected signal. To do this a program called MadGraph is used.
 449 MadGraph [22] starts with Feynman diagrams and then generates simulated events
 450 based on lots of different parameters.
 451 PYTHIA [23] is a package which adds the correct description of jets to MadGraph
 452 by including hadronization. The correct description of pile-up comes from other
 453 ATLAS software.
 454 The tool to access all this data and analyse it a tool called ROOT, which is used
 455 for programming high energy physics related tools [24].

2

Validation of smearing functions

458 A full detector simulation of the ATLAS detector based on the GEANT [25] pro-
459 gram makes it possible to obtain the expected detector responses to electrons,
460 muons, tau leptons, photons (γ) and jets of hadrons. However these simulations
461 are extremely time-consuming and require a lot of computing power. Also at the
462 present time only a limited set of these simulations exists for the ATLAS phase II
463 upgrade.

464 In this thesis a different strategy is used. Instead of performing a full detector
465 simulation the observed particles from the event generator, which simulates the
466 proton-proton collisions, are smeared by using random numbers following reso-
467 lution functions specific to each type of particle. These emulate how the detector
468 and the reconstruction is affected by the increased luminosity and the pile-up
469 which comes with this.

470 The resolution functions or smearing functions are the official functions devel-
471 oped from previous studies [1, 26] by the ATLAS collaboration for the study of
472 the ATLAS phase II upgrade. The key feature of those studies was that the di-
473 rection of the momenta is unaffected and that only jets and E_T^{Miss} are affected by
474 pile-up. Since this was confirmed in previous studies it was not incorporated into
475 the smearing functions as discussed more in section 2.1.

476 Since part of this thesis work was to take the official ATLAS smearing functions
477 and apply the smearing to each particle, it was important to check that the en-
478 ergy and momenta resolutions of the smeared objects were consistent with the
479 expected values. Thus in this chapter the energy and momenta resolutions are
480 measured after applying the smearing to some simulated processes and the re-
481 sulting resolutions are compared with the expected values.

482 2.1 Smearing functions

483 These smearing functions are designed so that they take into account the effi-
 484 ciency of the different detectors, limitations from how they are constructed as
 485 well as their dependence on pile-up. They also take into account how all this
 486 varies depending on the measured entries energy or momenta.

487 Terminology:

- 488 • Data before smearing, simulated data, is denoted as data at a truth level or
 489 truth data.
- 490 • Data after smearing, which is comparable to what is measured is denoted
 491 as reconstructed or reco data as discussed in subsection 1.3.4.

492 2.1.1 Electron and photon

493 The identification of electrons relies on finding an isolated electron track and
 494 a pattern in the calorimeter compatible with an electron shower. Pile-up will
 495 affect the electrons by decreasing the efficiency to identify an electron because of
 496 the increased number of tracks. However for the identified electrons the energy
 497 resolution will be close to that without pile-up.

498 The electron and photon have the same smearing since they are both detected in
 499 a similar way.

500 2.1.2 Muon

501 The identification of muons relies on isolated tracks in the inner detector being
 502 matched with information in the muon system. Since the muon system is the
 503 outer most detector seen from the collision point it is unaffected by the false
 504 detection effects of pile-up.

505 2.1.3 Tau

506 Tau is detected similarly to electron and photon. In this thesis all tau processes
 507 are assumed to be at 3 prong. Where prong refers to the different amount of
 508 tracks from which they were reconstructed. This in turn means that the effect of
 509 pile-up will be worse compared to an electron as a triplet must be found in an
 510 increased number of tracks.

511 2.1.4 Jets

512 The largest effect of pile-up is to add additional jets in the ATLAS detector. These
 513 additional jets contribute to additional energy deposited inside the existing jets
 514 and to E_T^{Miss} .

515 2.1.5 Missing Transversal Energy

516 E_T^{Miss} , the missing transversal energy, which was discussed in subsection 1.3.6,
 517 and defined in (1.9) is calculated by knowing that there should be energy conser-

518 vation in the collision. It is comprised of different parts, one from neutrinos, one
519 from errors in the other measurements and one from new physics. It should be
520 affected by pile-up as described above.

521 2.2 Validation

522 To validate the smearing functions a comparison with Ref. [26] was made where
 523 the standard deviation, depending on the energy or momentum value of an entity,
 524 was given, see section 2.4. This is performed using the simulated processes listed
 in table 2.1.

Table 2.1: Different processes from where data has been taken. Each sample is a simulation of a physical process, the simulation names can be found in appendix A

Particle	Process
Electron	$W \rightarrow e\nu$
Muon	$W \rightarrow \mu\nu$
Tau	$W \rightarrow \tau\nu$
γ	$\gamma + \text{Jet sample}$
Jets	Jet sample
E_T^{Miss}	$Z \rightarrow \nu\nu + \text{Jet sample}$

525

526 2.2.1 Method

527 The energy and momentum resolutions are obtained for each type of particle by
 528 comparing the values before and after smearing.

529 This is done by looking at the reco data for a given slice at a truth energy or mo-
 530 mentum value. Since the smearing functions takes a lot into account the match
 531 will not be a fine line as seen in figure 2.3b.

532 By fitting a Gaussian curve to this data will then result in the standard deviation
 533 which is used in the validation. The standard deviation is also known as the
 534 resolution of the data and will be denoted σ .

535 This resolution is then compared to previous results, [26].

536 To get enough statistics enough data must be available for a given truth energy
 537 or momenta and the analysis must be specific enough to only look at a narrow
 538 enough interval around this point.

539 Step by step method

- 540 • Take a MC sample with a given particle, i.e electrons.
- 541 • Choose a slice of electron which have a truth energy of a given value (75
 542 GeV for electrons).
- 543 • Plot the smeared electron energy for this slice of truth energy. Given for
 544 electrons and photons in figure 2.1.
- 545 • For this distribution of smeared energy, fit a Gaussian distribution and cal-
 546 culate the sigma value of this Gaussian.
- 547 • Compare this sigma, which is the calculated resolution to the expected res-
 548 olution given from the smearing functions.

549 2.3 Results

- 550 As discussed above, the method was to plot the data against its smeared counter-
551 part and through this determine σ to see if it conforms to the expected values.
- 552 Only one energy value is shown for simplicity, though the comparison was done
553 for different energy values.
- 554 The average number of pile-up is fixed at 60 as a benchmark unless anything else
555 is stated.
- 556 As the comparison, figure 2.4, figure 2.1, figure 2.2 and figure 2.5 are divided
557 depending on the different η values.
- 558 All results are summarized in table 2.5.

559 2.3.1 Electron and photon

560 Since these interact very similarly in the detector, their smearing functions are
 561 identical. The slice value represents at which value of unsmeared energy or mo-
 562 mentum this smearing occurs.

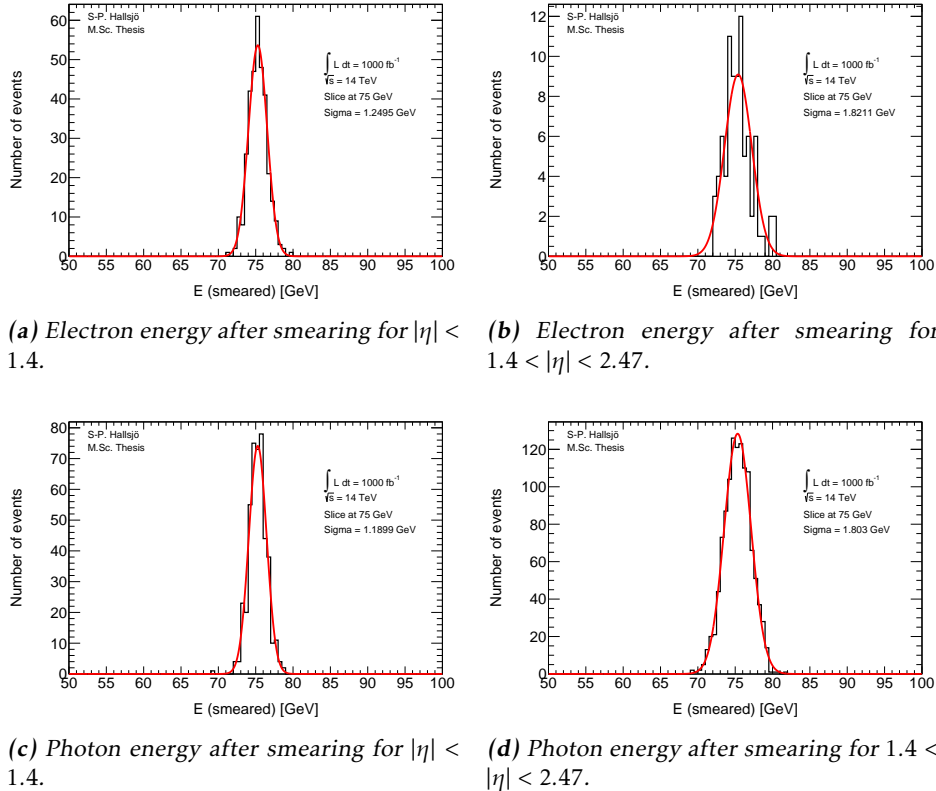
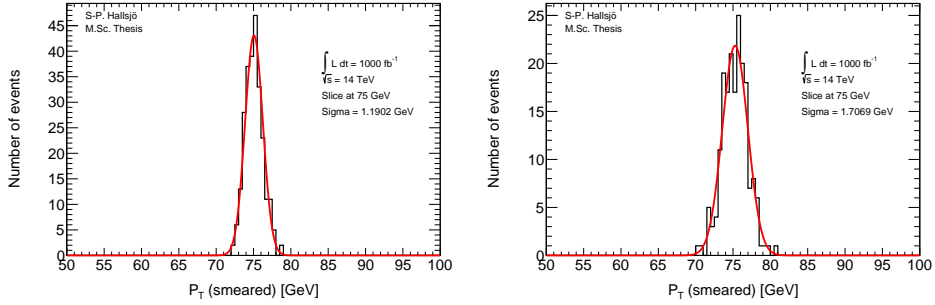


Figure 2.1: Photon and electron energy after smearing.

563 2.3.2 Muon

564 Since muons are shielded from the effects of pile-up only efficiency and detector
 565 limitations affect the smearing.

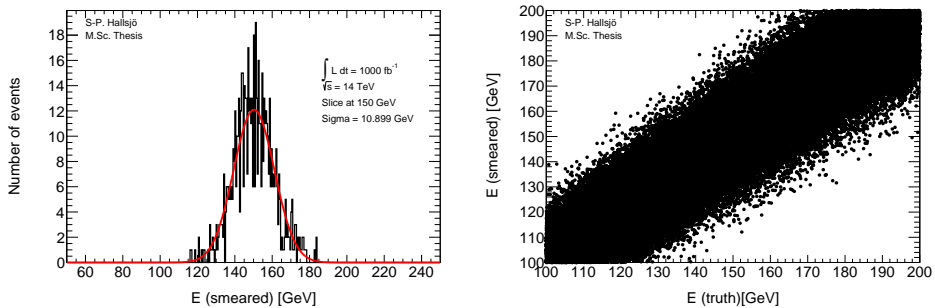


(a) Muon momenta after smearing for $|\eta| < 1.05$. (b) Muon momenta after smearing for $1.05 < |\eta|$.

Figure 2.2: Muon momenta after smearing.

566 2.3.3 Tau

567 As described in subsection 2.1.3 tauons are detected similarly to electrons and
 568 photons. Thus the plots should look similarly to those in the previous subsection
 569 apart from the slice being at 150 GeV. In figure 2.3a the Gaussian fit (red) and the
 570 data (black) are given for tau detected through 3 prong. In figure 2.3b smeared
 571 versus truth energy is shown.



(a) Tau energy after smearing.

(b) Tau energy vs smeared.

Figure 2.3: Tau energy after smearing and energy vs smearing.

2.3.4 Jets

Jets as described in subsection 1.3.6, are hadronic showers. The smearing functions are divided into four different regions depending on the angle η .

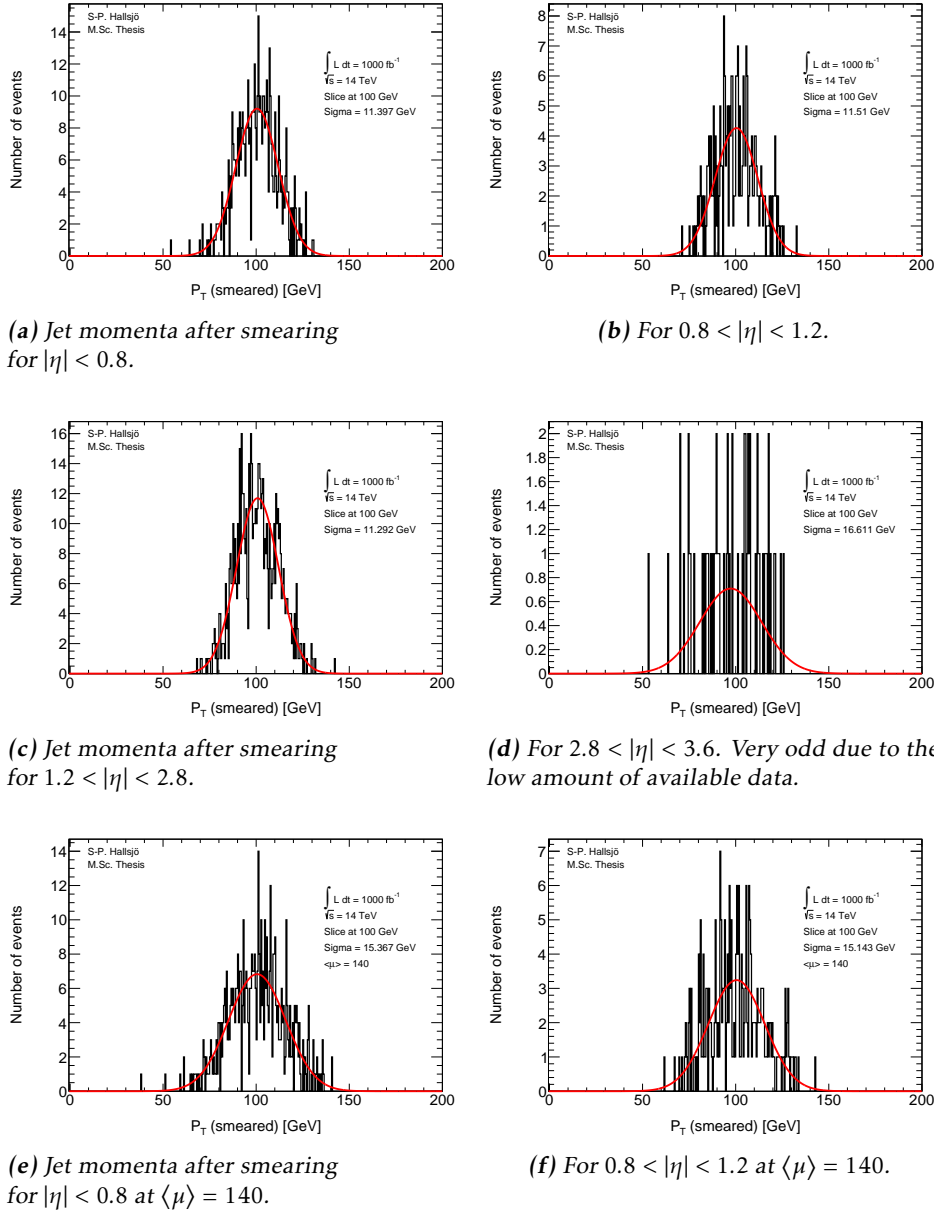


Figure 2.4: Jet momenta after smearing.

575 2.3.5 Missing Transversal Energy

576 The figures in this subsection are, compared to the above, given as absolute smear-
 577 ing, thus at 0 it represents that the energy is unsmeared, compared to the others
 578 where the slice value represents the unsmeared.

579 Here the E_T^{Miss} is projected down to the x- and y-axis, since these are the transver-
 580 sal axes, to be smeared.

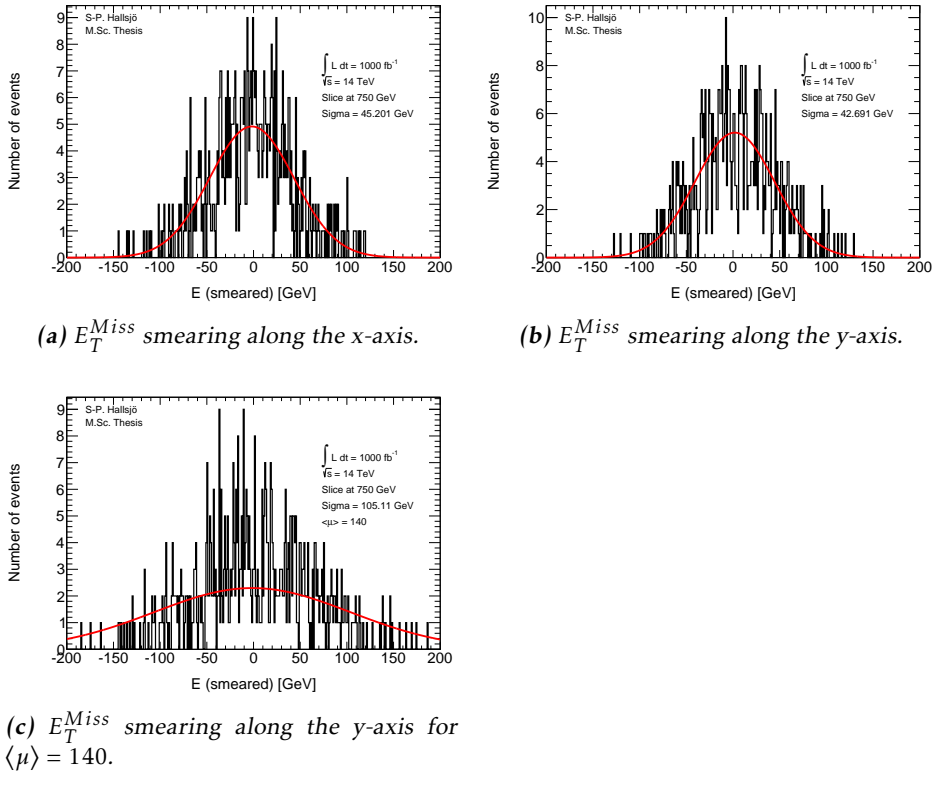


Figure 2.5: E_T^{Miss} smearing plots

581 2.4 Expected results

582 Since the leptons and photons are all detected by fitting detectors responses to
 583 different tracks, meaning that the effect of pile-up should be that there are more
 584 track to match, but it should not affect which ones are matched. The indepen-
 585 dence of pile-up for leptons and photons is backed up in previous research, for
 586 instance [1, 27].

587 To validate the smearing code, comparisons were made with [26] which gave the
 588 following formulation for the expected σ :

Observable	Absolute σ
Electron & photon	$\sigma = 0.3 \oplus 0.1\sqrt{E(GeV)} \oplus 0.01E(GeV), \eta < 1.4$ $\sigma = 0.3 \oplus 0.15\sqrt{E(GeV)} \oplus 0.015E(GeV), 1.4 < \eta < 2.47$
Muon momentum	$\sigma = \frac{\sigma_{id}\sigma_{ms}}{\sigma_{id} \oplus \sigma_{ms}}$ $\sigma_{id} = P_T(a_1 \oplus a_2 P_T)$ $\sigma_{ms} = P_T(\frac{b_0}{P_T} \oplus b_1 \oplus b_2 P_T)$
Tau energy	$\sigma = (0.03 \oplus \frac{0.76}{\sqrt{E(GeV)}})E(GeV), \text{for 3 prong.}$
Jet momentum	$\sigma = P_T(GeV)(\frac{N}{P_T} \oplus \frac{S}{\sqrt{P_T}} \oplus C)$ where $N = a(\eta) + b(\eta)\mu$
E_T^{Miss}	$\sigma = (0.4 + 0.09\sqrt{\mu})\sqrt{\sum E(GeV) + 20\mu}$

Table 2.2: Expected absolute σ where the parameters are given for muons in table 2.3 and for jets in table 2.4. Functions take from [26].

	a_1	a_2	b_0	b_1	b_2
$ \eta < 1.05$	0.01607	0.000307	0.24	0.02676	0.00012
$ \eta > 1.05$	0.03000	0.000387	0.00	0.03880	0.00016

Table 2.3: Parameters used in the muon smearing function taken from [26].

$ \eta $	a	b	s	C
0-0.8	3.2	0.07	0.74	0.05
0.8-1.2	3.0	0.07	0.81	0.05
1.2-2.8	3.3	0.08	0.54	0.05
2.8-3.6	2.8	0.11	0.83	0.05

Table 2.4: Parameters used in the jet smearing function taken from [26].

Process	σ [GeV]	Expected σ
Electron low η	1.25 ± 0.05	1.18
High η	1.82 ± 0.14	1.74
Photon low η	1.19 ± 0.04	1.18
High η	1.80 ± 0.04	1.74
Muon low η	1.19 ± 0.05	1.50
High η	1.71 ± 0.09	2.18
Tau	10.90 ± 0.31	10.34
Jet low η	11.40 ± 0.35	11.60
$\langle \mu \rangle = 140$	15.37 ± 0.47	15.77
Mid low η	11.51 ± 0.52	11.94
$\langle \mu \rangle = 140$	15.14 ± 0.68	15.95
Mid high η	11.29 ± 0.31	10.94
High η	16.61 ± 1.53	13.50
E_T^{Miss} x-axis	45.20 ± 1.35	48.45
E_T^{Miss} y-axis	42.69 ± 2.28	48.45
$\langle \mu \rangle = 140$	105.11 ± 12.24	87.28

Table 2.5: σ values.

- 589 • Where the given σ is still the absolute.
- 590 • Where the large difference between calculated and expected σ for Muons
591 and E_T^{Miss} is explained by incorrectly calculated errors in σ .

592 2.5 Discussion

593 2.5.1 Smearing independent on pile-up

594 From the validation done it was interesting to note that the smearing functions
595 were created from previous studies, [1, 27], which had shown that leptons and
596 photons are not affected by pile-up. This may seem incredible however it be-
597 comes quite logical when one understands how the detectors work. To be able to
598 detect particles the detectors must detect an excess of energy which comes from
599 a particle passing through. This should not be distorted by an increased pile-up.
600 The amount of particles passing through will of course increase, but the detec-
601 tions should be unaffected as well as the recreation of the events. However with
602 the same logic it makes sense that jets and E_T^{Miss} are quite affected since they
603 are combined of several parts, either hadronic particles or by all the transversal
604 missing energy.

605 Another interesting part is how the effect diminishes with and increasing energy.
606 As seen above, and through the the formula, for the high energies which were of
607 interest here the effect is minimal.

608 2.5.2 Comparison to expected results

609 One of the major problems in the comparison was to get the significance of the
610 Gaussian fit to be calculated correctly. The tool ROOT has a lot of different fea-
611 tures which made this task somewhat difficult. Also since this is a statistical
612 property there is a statistical fluctuation in the result.

613 Another was to retrieve the correct values from the paper, [26], since it was un-
614 clear if the values given were absolute or scale dependent. This has now been
615 corrected in a new version of the paper.

616 **2.6 Conclusion**

- 617 The smearing functions work as intended within 5.8 sigma, however when using
618 a test box and averaging the sigmas one ends up with half of this for the extreme
619 cases, muons and E_T^{Miss} y-axis.

620

3

621

Evaluating dark matter signals

622 **Disclaimer: All data provided is still a work in progress and may be subject to
623 change before the final version.**

624 The main goal of the thesis is to investigate if certain dark matter signals can
625 be detected after the high luminosity upgrade. One immediate worry is that the
626 background will be large in comparison to the signal, making the signal undetectable.
627

628 Another goal is to investigate if it might become more difficult to differentiate
629 between the signal and background due to the degradation of jet and missing
630 energy resolutions in the high luminosity upgrade.

631 This thesis focus on using a luminosity at 1000 fb^{-1} and a center of mass energy
632 at 14 TeV. The reco data is created using a pile-up rate, $\langle \mu \rangle = 140$ as expected
633 during phase II.

634 The signal models are given in appendix A along with the background models.
635 The different models were introduced subsection 1.2.5 and will be discussed in
636 more detail in this chapter.

637 Each signal model has been evaluated in different signal regions and the de-
638 tectability has been evaluated using a statistical P-value. This process has been
639 performed at a pile-up value of 140, as expected for after the high luminosity
640 upgrade.

641 3.1 Signal to background ratio

642 3.1.1 Signal Region

643 A signal region (SR) is defined as a set of selections on event variables designed
 644 to create a sample which is enriched in signal and depleted of background. One
 645 usually tries to design the signal region so that the signal is large enough and the
 646 background small enough that one would statistically be able to either:

- 647 • Exclude the signal if the observation of the data is compatible with a back-
 ground only hypothesis.
- 649 • Detect the signal and quantify the significance of the excess in data over
 650 background if the data is consistent with a signal + background hypothesis.

651 An event is a recorded proton-proton collision which consists of hundreds or
 652 thousands of observables such as the number of electrons, muons, jets, tau leptons,
 653 gammas or E_T^{Miss} each with their energy and momenta.

654 To define an optimal signal region is not known a priori and has to be studied for
 655 different signal models. The optimal region typically changes e.g with a change
 656 of the mass of new particles for instance the WIMP mass or the suppression scale.
 657 This is why there are several different signal regions to be studied in this thesis.

658 3.1.2 Weight

659 A weight is used to normalize different types of data so that they can be compared.
 660 As given in (1.7), the total number of events can be estimated as:

$$N = \sigma \int \mathcal{L} dt \equiv \sigma \mathcal{L} \quad (3.1)$$

661 Thus, if all events are generated at different luminosities, depending on the com-
 662 puting power of the computer which performed the simulation, the following
 663 weight should be used to receive the events at a new luminosity:

$$weight = \frac{\mathcal{L}\sigma}{N_{Raw}} \quad (3.2)$$

664 where N_{Raw} is the number of events expected at the luminosity that was set to cre-
 665 ate the data, compared to \mathcal{L} which is the luminosity at which the data is compared
 666 and σ is the cross-section. In this thesis the luminosity is fixed at $\mathcal{L} = 1000\text{fb}^{-1}$.

667 3.1.3 Verification of background normalization

668 To verify that the background samples are correctly normalized they are com-
 669 pared with Ref. [28] in which the center of mass energy is 8 TeV and the lumi-
 670 nosity is 10 fb^{-1} . Since the luminosity is not 1000 fb^{-1} as used in this thesis the
 671 expected values from the paper scaled up with a factor 100 to be comparable.

672 Somewhat unexpectedly a center of mass energy at 8 TeV had cross-sections a fac-
 673 tor 4 lower than the cross-sections at 14 TeV. These cross-sections are generated

either with MadGraph[22] or PYTHIA[23] depending on the generator given for each dataset in appendix A.

The signal regions used in the article were the following:

Selection Criteria		
Jet veto, require no more than 2 jets with $p_T > 30\text{GeV}$ and $ \eta < 4.5$		
Lepton veto, no electron or muon		
Leading jet with $ \eta < 2.0$ and $\Delta\phi(\text{jet}, E_T^{Miss}) > 0.5$ (second-leading jet)		
signal region	SR3p	SR4p
minimum leading jet p_T (GeV)	350	500
minimum E_T^{Miss} (GeV)	350	500

Table 3.1: The signal regions from Ref. [28].

The article [28] has in total four signal regions, unfortunately since the simulated events used in this thesis are filtered before the analysis only the two highest regions are comparable. This can be seen in table 3.3 in subsection 3.4.1.

3.1.4 Errors in data

To make a thorough analysis of the background it is important to take into consideration different errors that exist in the number of events. This is especially important when looking at which signals can be excluded in different signal regions. There exists three main types of errors:

- Statistical errors from MC.
- Statistical errors from the control region.
- Systematic errors.

The statistical errors from MC come from the method of generating background events and is unfortunately nothing that can be estimated when one is not generating the events.

The statistical errors from the control region require an explanation of what a control region is. A control region (CR) is similar to a signal region, a set of criteria which are imposed on the data. This criteria are not set so that there can be a region with almost no signal. In this CR there will still be fluctuations in the amount of background events due to statistical effects, which can then be measured.

The systematic errors is a fixed error which is always present coming from different approximations in how all the events were generated.

3.1.5 Figure of merit

To be able to evaluate different signal regions and different signal models, a figure of merit p is used. The value p is the probability for the background to fluctuate

to the value of the signal + background. Thus if the p-value is small, regardless if the signal is large or the background or its fluctuations are small, it is improbable that the background could result in the same value as if there was a signal and background. This means that for a sufficiently small p-value the signal is detectable.

Assuming the expected number of background events are $B \pm \sigma_B$ where σ_B is the quadratic sum of the statistical error from Monte Carlo, the statistical error from the control region (CR) and the systematic errors as explained in subsection 3.1.5. The expected number of signal events is S , assumed without fluctuation.

If no uncertainty in B or S is assumed, then the probability that the background will fluctuate up to the signal and background should follow a Poisson distribution as such:

$$P(S+B|B) = \frac{e^{-B} B^{(S+B)}}{(S+B)!} \quad (3.3)$$

The probability that the background will fluctuate to a value N larger or equal to the signal and background then becomes:

$$P(B \geq S+B|B) \equiv P(N|B) = \sum_{N=S+B}^{\infty} \frac{e^{-B} B^N}{N!} \quad (3.4)$$

However since there is an uncertainty in the background, the probability distribution $P(N|B)$ must be convoluted with a Gaussian function:

$$G(N_B|B, \sigma_B) = \frac{1}{\sigma_B \sqrt{2\pi}} e^{-\frac{(N_B-B)^2}{2\sigma_B^2}} \quad (3.5)$$

where N_B is the expected number of background events. The convolution is done using N_B as B resulting in the total probability density function:

$$\begin{aligned} F(N|N_B, \sigma_B) &= P(N|B)*G(N_B|B, \sigma_B) = \\ &= \int_{-\infty}^{\infty} P(N|N_B - B) G(N_B|B, \sigma_B) dN_B \end{aligned} \quad (3.6)$$

Inserting the sum over N leads to the probability of the background fluctuation to signal and background being obtained as.

$$p = \sum_{N=S+B}^{\infty} \int_{-\infty}^{\infty} P(N|N_B - B) G(N_B|B, \sigma_B) dN_B \quad (3.7)$$

In this thesis, two different models of the error in the background σ_B are used. Both models are based on Ref. [28]. As described in the beginning of this subsection the error is calculated as:

$$\sigma_B = \text{Statistical error from MC} \oplus \text{Statistical error in CR} \oplus \text{Systematic error}$$

- The statistical error from MC has been neglected since there is no way of estimating it.
- The statistical error from background CR has been taken from the article and assumed to decrease with the increased luminosity as, $\frac{30}{380} \frac{\sqrt{L_{old}}}{\sqrt{L_{new}}}$
- The systematic error has been given two different values, from the article: $\frac{30}{380}$ or fixed at 0.02.
- All this results the total error being used as either, 0.08 or 0.02.

3.1.6 D5 operator models

As described in subsection 1.2.5, one of the signals is modelled using the D5 operator. In this thesis two different scenarios are used, one at a dark matter mass of 50 GeV and one at 400 GeV.

Each of these models are modelled with a mass suppression scale, denoted M^* , which is connected to the cross-section of the process through:

$$\sigma_{new} = \frac{\sigma_{old}}{M^*} \quad (3.8)$$

In subsection 3.4.3 it is determined which values of M^* could be excluded with the upgraded LHC phase 2 upgrade and ATLAS.

3.1.7 Light vector mediator models

As described in subsection 1.2.5, the other signal model is a vector mediator model. In this thesis these signals have two different width scenarios and a number of different mediator mass scenarios. **Where width is related to the lifetime of the dark matter particle.** In addition to this there are, as with the D5 operator, two different dark matter masses, one at 50 GeV and one at 400 GeV.

The result of the investigation of which models are excludable with the upgraded LHC phase 2 upgrade and ATLAS are given in subsection 3.4.4.

3.2 Signal region definitions

3.2.1 Signal regions

To be able to compare signal results to previous papers new signal regions were devised. It was also discovered that the requirement of no electrons or muons was to harsh for the signal models. Because of this new signal criteria were devised.

Selection Criteria					
Jet veto, require no more than 2 jets with $p_T > 30\text{GeV}$ and $ \eta < 4.5$					
Lepton veto, no electron or muon.					
The electron veto is defined: $\Delta R(jet^{lead}, electron^{lead}) \geq 0.4$ and $electron^{lead} p_T > 20\text{GeV}$ removed.					
The muon veto is defined: $\Delta R(jet^{lead}, muon^{lead}) \geq 0.4$ and $muon^{lead} p_T > 20\text{GeV}$ removed.					
Leading jet with $ \eta < 2.0$ and $\Delta\phi(jet, E_T^{Miss}) > 0.5$ (second-leading jet)	SR1	SR1p	SR2	SR3	SR4
signal region	SR1	SR1p	SR2	SR3	SR4
minimum leading jet p_T (GeV)	350	500	600	800	1000
minimum E_T^{Miss} (GeV)	350	500	600	800	1000
signal region	SRa	SRb	SRc	SRd	
minimum leading jet p_T (GeV)	350	350	350	350	
minimum E_T^{Miss} (GeV)	350	600	800	1000	

Table 3.2: The new signal regions

3.2.2 Verifying background data

To make sure that the altered electron veto still produces results comparable with [28] a comparison is made again. This can be seen in subsection 3.4.1 in table 3.4.

3.3 Mitigating the effect of the high luminosity

As discussed in subsection 2.5.1 the smearing functions effect of pile-up should be minimal in the high energy regions which are of interest in this thesis.

From the formulation of the smearing functions, the biggest effect should be seen at low energies. This is related to the difficulty for the hardware triggers to select events. This means that one drawback of the high luminosity upgrade is that very low energy signal regions will be lost.

The effect of the high luminosity is seen in chapter 3.4 and discussed in subsection 3.5.2.

760 3.4 Results

761 3.4.1 Verifying background data

762 In table 3.3 and table 3.4 a comparison has been made between the number of
 763 simulated background events at a truth level and the number of expected events
 764 by scaling up the values from Ref. [28] by a factor 100. Truth data was used to
 765 not let the increased pile-up value affect the comparison. It can be seen that the
 766 simulated events and expected events coincide quite well on all accounts apart
 767 from $W \rightarrow \tau\nu$, $W \rightarrow \mu\nu$ and thus the total as well.

768 The difference in $W \rightarrow \tau\nu$ can be explained by the fact that τ can not be recreated
 769 as a jet in the simulated events which it can in measured events.

770 The difference in $W \rightarrow \mu\nu$ is explained through the simulated events having a
 771 better separation of muons neutrinos and E_T^{Miss} .

Process	SR3p		SR4p	
	Simulated	From paper	Simulated	From paper
$Z \rightarrow \nu\nu$	140298	152000	25250	27000
$W \rightarrow \tau\nu$	40701	37000	5862	3900
$W \rightarrow e\nu$	11229	11200	1507	1600
$W \rightarrow \mu\nu$	13727	15800	1872	4200
Total background	205955	218000	34491	36700

Table 3.3: Comparison of the simulated and expected events from Ref. [28] with $\mathcal{L} = 1000\text{fb}^{-1}$, cross-sections corresponding to $\sqrt{s} = 8\text{TeV}$ and using the same electron and muon veto.

Process	SR1		SR1p	
	Simulated	From paper	Simulated	From paper
$Z \rightarrow \nu\nu$	150753	152000	27569	27000
$W \rightarrow \tau\nu$	49320	37000	7318	3900
$W \rightarrow e\nu$	18329	11200	2534	1600
$W \rightarrow \mu\nu$	22290	15800	3218	4200
Total background	240690	218000	40639	36700

Table 3.4: Comparison of the simulated and expected events from Ref. [28] with $\mathcal{L} = 1000\text{fb}^{-1}$, cross-sections corresponding to $\sqrt{s} = 8\text{TeV}$ and using a modified electron and muon veto.

772 3.4.2 Events

773 In the following tables the number of events are given using one of the D5 opera-
 774 tors as the signal, and the background in the different signal regions. The number
 775 of background events is also used for the vector mediator signals.

Process at $\sqrt{s} = 14\text{TeV}$	SR1	SR2	SR3	SR4	SRa	Srb	Src	Srd
D5, mDm=50 GeV, M*=1TeV	129863	30219	10750	4391	129863	36410	12927	5221
Z $\rightarrow \nu\nu$	604479	42657	8424	2111	604479	58614	11383	2843
W $\rightarrow \tau\nu$	154140	7807	1308	295	154140	10679	1788	386
W $\rightarrow e\nu$	61772	2890	485	110	61772	3961	654	152
W $\rightarrow \mu\nu$	49114	2357	379	91	49114	3052	499	108
Total background	869505	55711	10597	2607	869505	76305	14325	3489

Table 3.5: Signal and background events for truth data in the signal regions.

Process at $\sqrt{s} = 14\text{TeV}$	SR1	SR2	SR3	SR4	SRa	Srb	SRc	SRd
D5, mDm=50 Gev, M*=1TeV	120295	28019	9978	4130	120295	38762	13752	5505
Z $\rightarrow \nu\nu$	553735	39105	7681	1932	553735	71613	13145	3140
W $\rightarrow \tau\nu$	156023	7741	1282	276	156023	14500	2174	467
W $\rightarrow e\nu$	58874	2706	448	106	58874	5177	790	176
W $\rightarrow \mu\nu$	47801	2299	380	89	47801	4031	618	139
Total background	816433	51850	9791	2404	816433	95322	16727	3922

Table 3.6: Signal and background events for reco data with $\langle \mu \rangle = 140$ in the signal regions.

776 Values need to be updated.

777 Note how the ratio between the number of signal events and total background increases from the first to the last signal regions
 778 meaning that these are good choices of signal regions. Also note how similar the two tables are even though table 3.6 is at reco
 779 with a pile-up rate of 140.

3.4.3 Limit on M*

For the D5 operators as described in subsection 3.1.6 limits on the mass suppression has been calculated by evaluating at which point the signal is covered by the background, meaning that the p-value > 0.05 . This is done using the two different error models as described in subsection 3.1.5 as figures of merit.

The limit is found, seen as a horizontal line in both figure 3.1 and figure 3.2, when the p-value = 0.05. Will insert new images

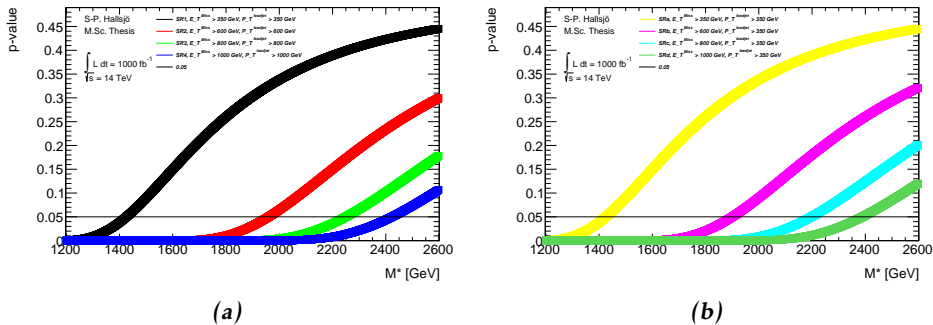


Figure 3.1: Limits of the mass suppression on a truth level for error model 0.02.

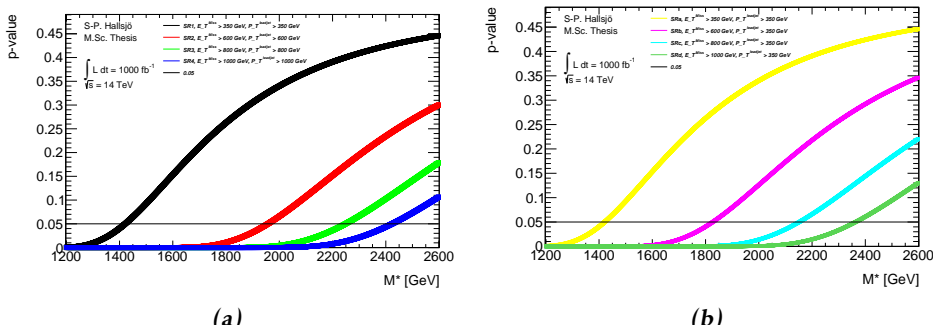


Figure 3.2: Limits of the mass suppression on a reco level for error model 0.02

Calculating the intersection between these lines and 0.05 results in, tables 3.7-3.10 for both a dark matter mass of 50 GeV and at 400 GeV at the different error models

What should be noted from these tables is the significant difference between the different signals regions, especially between 4 and d which are similar apart from

Signal region	Truth [GeV]	Reco [GeV]
SR1, symmetric 350	1425	1420
SR2, 600	1960	1957
SR3, 800	2249	2248
SR4, 1000	2423	2423
SRa, symmetric 350	1425	1421
SRb, asymmetric 600	1900	1827
SRc, 800	2197	2152
SRd, 1000	2389	2363

Table 3.7: Limits on mass suppression scales in GeV given for $mDm=50$ GeV and the 0.02 error model.

Signal region	Truth [GeV]	Reco [GeV]
SR1	1015	1012
SR2	1400	1400
SR3	1636	1637
SR4	1846	1854
SRa	1015	1012
SRb	1356	1303
SRc	1589	1553
SRd	1796	1768

Table 3.8: Limits on mass suppression scales in GeV given for $mDm=50$ GeV and the 0.08 error model.

Signal region	Truth [GeV]	Reco [GeV]
SR1, symmetric 350	1350	1346
SR2, 600	1871	1870
SR3, 800	2185	2186
SR4, 1000	2353	2322
SRa, symmetric 350	1350	1346
SRb, asymmetric 600	1814	1745
SRc, 800	2134	2087
SRd, 1000	2313	2281

Table 3.9: Limits on mass suppression scales in GeV given for $mDm=400$ GeV and the 0.02 error model.

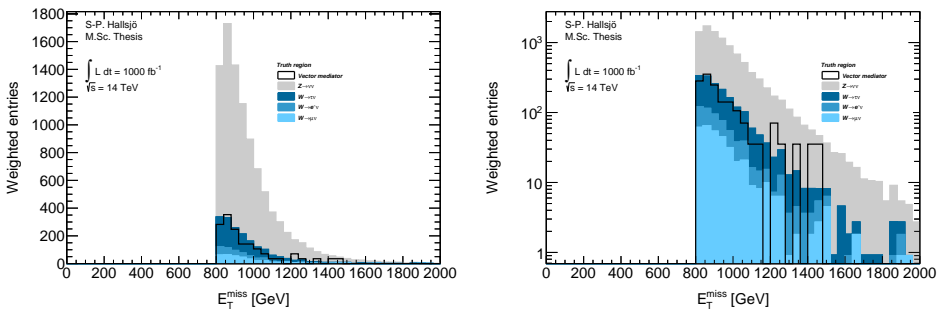
the lead jet cut. Also how small the effect from pile-up seems to be and the increase in dark matter mass.
 792
 793

Signal region	Truth [GeV]	Reco [GeV]
SR1	961	959
SR2	1337	1337
SR3	1589	1592
SR4	1793	1777
SRa	961	959
SRb	1295	1245
SRc	1544	1507
SRd	1739	1707

Table 3.10: Limits on mass suppression scales in GeV given for $mDm=400$ GeV and the 0.08 error model.

3.4.4 Limit on mediator mass

For the vector mediator modes as described in subsection 3.1.7 limits on which models can be excluded have been calculated. This is done by calculating which models the p-value is < 0.05 . This is done using the two different error models as described in subsection 3.1.5 as figures of merit. All signals which have been used can be found in A.2.3.



(a) Signal on background plot for E_T^{miss} on the reco level in SR3. **(b)** The same as a) with log scale on the y-axis

Figure 3.3: Signal on background plot to illustrate the a general plot. (OLD)

To set a limit on the mediator mass the p-value is calculated in different signal regions for the different signal models with different mediator mass. This resulted in the following plot.

Should be plots as in presentation with increasing mediator mass on x-axis and p-value as y-axis.

The limit is found when the p-value = 0.05.

What can be seen in the plots and in the tables is that the models are very robust

width	mDM=50 GeV	mDM=400 GeV
m/3	1000 GeV	1000 GeV
m/8p	3000 GeV	3000 GeV

Table 3.11: Limits on which the highest mediator mass which can be excluded for different widths, different dark matter masses for truth and reco and both error models. In SR2, 3, 4, c, d.

width	mDM=50 GeV	mDM=400 GeV
m/3	1000 GeV	1000 GeV
m/8p	1000 GeV	1000 GeV

Table 3.12: Limits on which the highest mediator mass which can be excluded for different widths, different dark matter masses for truth and reco and both error models. In SRb.

when it comes to increased fluctuation in the background as indicated by the error models and with the introduction of pile-up. It is though quite interesting to see that SRb is the signal region which was worst suited for the vector mediator signals. Which by looking at the definition would suggest that the background is less susceptible to a lead jet cut than the signals.

3.5 Discussion

3.5.1 Comparison to previous results

The background was compared to Ref. [28] altering the cross-sections of the samples used in this thesis to simulate a center of mass energy of 8 TeV instead of 14. This could unfortunately not be done for the signals as that would require new samples to be produced. As seen and some what discussed in subsection 3.4.1 the events corresponded quite nicely to the values from the paper. The discrepancies are explained by general differences between simulations and measured events, such as:

- The difference in $W \rightarrow \tau\nu$ can be explained by the fact that τ can not be recreated as a jet in the simulated events which it can in measured events.
- The difference in $W \rightarrow \mu\nu$ is explained through the simulated events having a better separation of muons neutrinos and E_T^{Miss} .

Where the choice of a new muon veto giving more events supports the final claim.

In table 3.13 the limits for the mass suppression scale are given from both the paper and from this work. It is seen that the increase in luminosity and center of mass energy gives an increase of the mass suppression scale by a factor of 2-3.

Dark matter mass	From simulation	From paper
50 GeV	1960 GeV	800 GeV
400 GeV	1871 GeV	700 GeV

Table 3.13: M^* values in SR2 from both simulation at 14 TeV, 1000fb^{-1} and from Ref. [28] at 8 TeV and 10fb^{-1} .

The whole discussion with Steven and David. **How should this be used? They have no public results.**

Difference to the previous estimates may be explained by:

- Them using lower cross-sections for the background.
- The difference in treatment of CB.

3.5.2 Effect of the high luminosity

As seen in section 3.4, the effect of a pile-up rate of 140 is minute in the signal regions chosen. The primary focus of this thesis was to look at the effect of pile-up, and try to mitigate the effect of it. However it is shown here that by choosing signal regions with a high enough requirement the effect is minute. Thus the focus was shifted to perform a more in-depth mono-jet analysis of different Dm signal models. These models were specifically the vector mediators.

For the mass suppression scale, as seen in subsection 3.4.3, comparing the truth values against the reco values the difference is at most $< 5\%$. Thus these signal

843 regions are preferable for use in the high luminosity upgrade.

844 Regarding the mediator models, as discussed in subsection 3.4.4 the models are
845 sensitive to exclusion regardless of truth or reco. This suggests that the different
846 models are very robust or that the effect of pile-up is negligible. However the
847 later is more probable since a tougher error model produces the same results.

848 3.6 Conclusion**849 3.6.1 Limit on M^***

850 The limits can be found in subsection 3.4.3 and are 2-3 times better than previous
851 results at 8 TeV and 10fb^{-1} .

852 3.6.2 Limit on mediator mass

853 The limits can be found in subsection 3.4.4 and is the first result done with these
854 models and thus can not be compared.

855 3.6.3 Effect of the high luminosity

856 At a pile-up level of 140 the effect is at most < 5% for the mass suppression scale
857 and does not affect the vector mediator models which are robust as discussed in
858 subsection 3.5.2.

859

4

860

Results and Conclusions

861 **Disclaimer: This chapter is not yet complete.**

862 4.1 Validation of smearing functions

863 Have some discussion.

864 Result they appear to work as expected, the reference paper was a bit unclear, I
865 leave my writing as a better reference.

4.2 Signal to background ratio

866 4.2.1 Limit on M^*

868 4.2.2 Limit on mediator mass

869 4.3 Other selection criteria and observables

870 4.3.1 Limit on M^*

871 4.3.2 Limit on mediator mass

872 4.4 Mitigating the effect of the high luminosity

873 4.5 Recommendations to mitigate the effect of the 874 high luminosity

875 Keep to a higher energy region, or signal region.

876 4.6 Suggestions for future research

877 With more time, search for new signal regions, the only solution now for the HL
878 is to go up in energy. Since none of the other parameters (eta,phi etc) seem to be
879 altered these can not be used. Is there something that has been overlooked?

880 Test the effect of pile-up for lower signal regions? See if the effect is as big as
881 predicted.

882 Explore other theoretical models for dark matter, other d operators etc. Models
883 that are based on Supersymmetry and not just effective theories.

884 Create more similar signal regions to be able to compare to the 20fb paper.

885 Sätt av ett kort kapitel sist i rapporten till att avrunda och föreslå räkningar för
886 framtida utveckling av arbetet.

887 Saving as reference. test citing as: Here we cite Duck [29] [29].

888 If the above works, remember to edit myreferences.

Appendix

890

A

891

Datasets

892 **Disclaimer: This appendix is not yet complete.**

893 **A.1 Background processes**

894 All datasets used are d4pd which is a dataformat used at CERN.

895 **A.1.1 Validation**

896 For the validation the following datasets were used, with a filter at generator level
897 at 450GeV for lead jet and MET.

898 157539 sherpa ct10 znunupt280 157534 sherpa ct10 wenupt200

899 157535 sherpa ct10 wmunupt200

900 157536 sherpa ct10 wtaunupt200

901 129160 pythia8 au2cteq6l1 perf jf17

902 129160 pythia8 au2cteq6l1 perf jf17

903 129170 pythia8 au2cteq6l1 gammajet dp17

904 They should be read as such: Monte Carlo version, dataset number, generator, ?
905 name.

906 **A.1.2 Background to signals**

907 The same as the above though now with the filter as indicated by their name. The
908 second znunu sample has been generated with and center of mass energy at 8
909 TeV.

910 157539 sherpa ct10 znunupt280

911 157539 8tev sherpa ct10 znunupt280

```

912 157536 sherpa ct10 wtaunupt200
913 157534 sherpa ct10 wenupt200
914 157535 sherpa ct10 wmunupt200

```

915 A.2 Signals

916 A.2.1 Qcut

917 Qcut means that the original data has been split into different parts depending
 918 on the value of the lead jet pt.

919 A.2.2 D5 signal processes

```

920 188408 madgraphpythia auet2bcteq6l1 d5 dm50 ms10000 qcut200
921 188409 madgraphpythia auet2bcteq6l1 d5 dm50 ms10000 qcut400
922 188410 madgraphpythia auet2bcteq6l1 d5 dm50 ms10000 qcut600
923 188411 madgraphpythia auet2bcteq6l1 d5 dm400 ms10000 qcut200
924 188412 madgraphpythia auet2bcteq6l1 d5 dm400 ms10000 qcut400
925 188413 madgraphpythia auet2bcteq6l1 d5 dm400 ms10000 qcut600

```

926 All signals should be read as such: Monte Carlo version, dataset number, generator, ?, name of operator, dark matter mass, default mass suppression scale,
 927 qcut part. As discussed in reference
 928

929 A.2.3 Light vector mediator processes

```

930 188414 madgraphpythia auet2bcteq6l1 dmv dm50 mm100 w3 qcut200
931 188422 madgraphpythia auet2bcteq6l1 dmv dm50 mm100 w3 qcut400
932 188430 madgraphpythia auet2bcteq6l1 dmv dm50 mm100 w3 qcut600
933 188415 madgraphpythia auet2bcteq6l1 dmv dm50 mm300 w3 qcut200
934 188423 madgraphpythia auet2bcteq6l1 dmv dm50 mm300 w3 qcut400
935 188431 madgraphpythia auet2bcteq6l1 dmv dm50 mm300 w3 qcut600
936 188416 madgraphpythia auet2bcteq6l1 dmv dm50 mm500 w3 qcut200
937 188424 madgraphpythia auet2bcteq6l1 dmv dm50 mm500 w3 qcut400
938 188432 madgraphpythia auet2bcteq6l1 dmv dm50 mm500 w3 qcut600
939 188417 madgraphpythia auet2bcteq6l1 dmv dm50 mm1000 w3 qcut200
940 188425 madgraphpythia auet2bcteq6l1 dmv dm50 mm1000 w3 qcut400
941 188433 madgraphpythia auet2bcteq6l1 dmv dm50 mm1000 w3 qcut600
942 188418 madgraphpythia auet2bcteq6l1 dmv dm50 mm3000 w3 qcut200
943 188426 madgraphpythia auet2bcteq6l1 dmv dm50 mm3000 w3 qcut400
944 188434 madgraphpythia auet2bcteq6l1 dmv dm50 mm3000 w3 qcut600
945 188419 madgraphpythia auet2bcteq6l1 dmv dm50 mm6000 w3 qcut200
946 188427 madgraphpythia auet2bcteq6l1 dmv dm50 mm6000 w3 qcut400
947 188435 madgraphpythia auet2bcteq6l1 dmv dm50 mm6000 w3 qcut600

```

```
948 188420 madgraphpythia auet2bcteq6l1 dmv dm50 mm10000 w3 qcut200
949 188428 madgraphpythia auet2bcteq6l1 dmv dm50 mm10000 w3 qcut400
950 188436 madgraphpythia auet2bcteq6l1 dmv dm50 mm10000 w3 qcut600
951 188421 madgraphpythia auet2bcteq6l1 dmv dm50 mm15000 w3 qcut200
952 188429 madgraphpythia auet2bcteq6l1 dmv dm50 mm15000 w3 qcut400
953 188437 madgraphpythia auet2bcteq6l1 dmv dm50 mm15000 w3 qcut600
954 188438 madgraphpythia auet2bcteq6l1 dmv dm50 mm100 w8pi qcut200
955 188446 madgraphpythia auet2bcteq6l1 dmv dm50 mm100 w8pi qcut400
956 188454 madgraphpythia auet2bcteq6l1 dmv dm50 mm100 w8pi qcut600
957 188439 madgraphpythia auet2bcteq6l1 dmv dm50 mm300 w8pi qcut200
958 188447 madgraphpythia auet2bcteq6l1 dmv dm50 mm300 w8pi qcut400
959 188455 madgraphpythia auet2bcteq6l1 dmv dm50 mm300 w8pi qcut600
960 188440 madgraphpythia auet2bcteq6l1 dmv dm50 mm500 w8pi qcut200
961 188448 madgraphpythia auet2bcteq6l1 dmv dm50 mm500 w8pi qcut400
962 188456 madgraphpythia auet2bcteq6l1 dmv dm50 mm500 w8pi qcut600
963 188441 madgraphpythia auet2bcteq6l1 dmv dm50 mm1000 w8pi qcut200
964 188449 madgraphpythia auet2bcteq6l1 dmv dm50 mm1000 w8pi qcut400
965 188457 madgraphpythia auet2bcteq6l1 dmv dm50 mm1000 w8pi qcut600
966 188442 madgraphpythia auet2bcteq6l1 dmv dm50 mm3000 w8pi qcut200
967 188450 madgraphpythia auet2bcteq6l1 dmv dm50 mm3000 w8pi qcut400
968 188458 madgraphpythia auet2bcteq6l1 dmv dm50 mm3000 w8pi qcut600
969 188444 madgraphpythia auet2bcteq6l1 dmv dm50 mm10000 w8pi qcut200
970 188452 madgraphpythia auet2bcteq6l1 dmv dm50 mm10000 w8pi qcut400
971 188460 madgraphpythia auet2bcteq6l1 dmv dm50 mm10000 w8pi qcut600
972 188445 madgraphpythia auet2bcteq6l1 dmv dm50 mm15000 w8pi qcut200
973 188453 madgraphpythia auet2bcteq6l1 dmv dm50 mm15000 w8pi qcut400
974 188461 madgraphpythia auet2bcteq6l1 dmv dm50 mm15000 w8pi qcut600
975 188462 madgraphpythia auet2bcteq6l1 dmv dm400 mm500 w3 qcut200
976 188468 madgraphpythia auet2bcteq6l1 dmv dm400 mm500 w3 qcut400
977 188474 madgraphpythia auet2bcteq6l1 dmv dm400 mm500 w3 qcut600
978 188463 madgraphpythia auet2bcteq6l1 dmv dm400 mm1000 w3 qcut200
979 188469 madgraphpythia auet2bcteq6l1 dmv dm400 mm1000 w3 qcut400
980 188475 madgraphpythia auet2bcteq6l1 dmv dm400 mm1000 w3 qcut600
981 188464 madgraphpythia auet2bcteq6l1 dmv dm400 mm3000 w3 qcut200
982 188470 madgraphpythia auet2bcteq6l1 dmv dm400 mm3000 w3 qcut400
983 188476 madgraphpythia auet2bcteq6l1 dmv dm400 mm3000 w3 qcut600
984 188465 madgraphpythia auet2bcteq6l1 dmv dm400 mm6000 w3 qcut200
985 188471 madgraphpythia auet2bcteq6l1 dmv dm400 mm6000 w3 qcut400
986 188477 madgraphpythia auet2bcteq6l1 dmv dm400 mm6000 w3 qcut600
```

```
987 188466 madgraphpythia auet2bcteq6l1 dmv dm400 mm10000 w3 qcut200
988 188472 madgraphpythia auet2bcteq6l1 dmv dm400 mm10000 w3 qcut400
989 188478 madgraphpythia auet2bcteq6l1 dmv dm400 mm10000 w3 qcut600
990 188467 madgraphpythia auet2bcteq6l1 dmv dm400 mm15000 w3 qcut200
991 188473 madgraphpythia auet2bcteq6l1 dmv dm400 mm15000 w3 qcut400
992 188479 madgraphpythia auet2bcteq6l1 dmv dm400 mm15000 w3 qcut600
993 188480 madgraphpythia auet2bcteq6l1 dmv dm400 mm500 w8pi qcut200
994 188486 madgraphpythia auet2bcteq6l1 dmv dm400 mm500 w8pi qcut400
995 188492 madgraphpythia auet2bcteq6l1 dmv dm400 mm500 w8pi qcut600
996 188481 madgraphpythia auet2bcteq6l1 dmv dm400 mm1000 w8pi qcut200
997 188487 madgraphpythia auet2bcteq6l1 dmv dm400 mm1000 w8pi qcut400
998 188493 madgraphpythia auet2bcteq6l1 dmv dm400 mm1000 w8pi qcut600
999 188482 madgraphpythia auet2bcteq6l1 dmv dm400 mm3000 w8pi qcut200
1000 188488 madgraphpythia auet2bcteq6l1 dmv dm400 mm3000 w8pi qcut400
1001 188494 madgraphpythia auet2bcteq6l1 dmv dm400 mm3000 w8pi qcut600
1002 188483 madgraphpythia auet2bcteq6l1 dmv dm400 mm6000 w8pi qcut200
1003 188489 madgraphpythia auet2bcteq6l1 dmv dm400 mm6000 w8pi qcut400
1004 188495 madgraphpythia auet2bcteq6l1 dmv dm400 mm6000 w8pi qcut600
1005 188484 madgraphpythia auet2bcteq6l1 dmv dm400 mm10000 w8pi qcut200
1006 188490 madgraphpythia auet2bcteq6l1 dmv dm400 mm10000 w8pi qcut400
1007 188496 madgraphpythia auet2bcteq6l1 dmv dm400 mm10000 w8pi qcut600
1008 188485 madgraphpythia auet2bcteq6l1 dmv dm400 mm15000 w8pi qcut200
1009 188491 madgraphpythia auet2bcteq6l1 dmv dm400 mm15000 w8pi qcut400
1010 188497 madgraphpythia auet2bcteq6l1 dmv dm400 mm15000 w8pi qcut600
```

1011
1012

Bibliography

- 1013 [1] Collaboration ATLAS. Letter of Intent for the Phase-II Upgrade of the
1014 ATLAS Experiment. Dec 2012. URL [https://cds.cern.ch/record/](https://cds.cern.ch/record/1502664/)
1015 1502664/. Cited on pages 1, 17, 26, and 28.
- 1016 [2] B.H. Bransden and C.J. Joachain. *Quantum mechanics*. Pearson Education,
1017 second edition, 2000. Cited on page 3.
- 1018 [3] Sven-Patrik Hallsjö. Covering the sphere with noncontextuality inequal-
1019 ities. Bachelor's thesis, Linköping University, The Institute of Technol-
1020 ogy, 2013. URL [http://urn.kb.se/resolve?urn=urn:nbn:se:liu:](http://urn.kb.se/resolve?urn=urn:nbn:se:liu:diva-103663)
1021 diva-103663. Cited on page 3.
- 1022 [4] A. Zee. *Quantum Field Theory in a Nutshell*. Princeton University Press,
1023 illustrated edition edition, March 2003. ISBN 0691010196. Cited on pages
1024 3, 6, and 7.
- 1025 [5] Herbert Goldstein, Charles P. Poole, and John L. Safko. *Classical Mechanics*
1026 (*3rd Edition*). Addison-Wesley, 3 edition, June 2001. ISBN 0201657023.
1027 Cited on page 3.
- 1028 [6] W. E. Burcham and M. Jobes. *Nuclear and Particle Physics*. Pearson educa-
1029 tion, second edition, 1995. Cited on page 4.
- 1030 [7] The ATLAS Collaboration. Observation of a new particle in the search
1031 for the Standard Model Higgs boson with the ATLAS detector at the LHC.
1032 *Phys. Lett. B*, 716(arXiv:1207.7214). CERN-PH-EP-2012-218):1–29. 39 p,
1033 Aug 2012. Cited on page 4.
- 1034 [8] Standard model of elementary particles. [http://en.wikipedia.org/](http://en.wikipedia.org/wiki/File:Standard_Model_of_Elementary_Particles.svg)
1035 [wiki/File:Standard_Model_of_Elementary_Particles.svg](http://en.wikipedia.org/wiki/File:Standard_Model_of_Elementary_Particles.svg),
1036 2014. Accessed: 2014-03-24. Cited on page 4.
- 1037 [9] G. Jungman, M. Kamionkowski, and K. Griest. Supersymmetric dark matter.
1038 *Physics Reports*, 267:195–373, March 1996. doi: 10.1016/0370-1573(95)
1039 00058-5. Cited on pages 4 and 5.

- 1040 [10] NASA. NASA's solar system exploration: the planets: orbits and
1041 physical characteristics. <https://solarsystem.nasa.gov/planets/>
1042 charchart.cfm, 2014. Accessed: 2014-03-21. Cited on page 6.
- 1043 [11] T. S. van Albada, J. N. Bahcall, K. Begeman, and R. Sancisi. Distribution
1044 of dark matter in the spiral galaxy NGC 3198. *Astrophysical Journal*, 295:
1045 305–313, August 1985. doi: 10.1086/163375. Cited on page 6.
- 1046 [12] Jessica Goodman, Masahiro Ibe, Arvind Rajaraman, William Shepherd,
1047 Tim M.P. Tait, et al. Constraints on Light Majorana dark Matter from Collid-
1048 ers. *Phys.Lett.*, B695:185–188, 2011. doi: 10.1016/j.physletb.2010.11.009.
1049 Cited on pages 5 and 7.
- 1050 [13] ATLAS Collaboration. Search for dark matter candidates and large extra di-
1051 mensions in events with a jet and missing transverse momentum with the at-
1052 las detector. *J. High Energy Phys.*, 04(arXiv:1210.4491. CERN-PH-EP-2012-
1053 210):075. 58 p, October 2012. URL [http://cds.cern.ch/record/](http://cds.cern.ch/record/1485031)
1054 1485031. Cited on pages 5, 8, and 9.
- 1055 [14] J. Goodman, M. Ibe, A. Rajaraman, W. Shepherd, T. M. P. Tait, and H.-B. Yu.
1056 Constraints on dark matter from colliders. *Phys.Rev.D82:116010,2010*, 82
1057 (11):116010, December 2010. doi: 10.1103/PhysRevD.82.116010. Cited on
1058 page 7.
- 1059 [15] ATLAS. Atlas luminosity public results. <https://twiki.cern.ch/twiki/bin/view/AtlasPublic/LuminosityPublicResults>, 2013.
1060 Accessed: 2014-03-06. Cited on page 10.
- 1061 [16] AC Team. The four main LHC experiments, Jun 1999. URL <http://cds.cern.ch/record/40525>. Cited on page 10.
- 1062 [17] Werner Herr and B Muratori. Concept of luminosity. 2006. URL <http://cds.cern.ch/record/941318/>. Cited on page 11.
- 1063 [18] The ATLAS Collaboration. The atlas experiment at the cern large hadron col-
1064 linder. *Journal of Instrumentation*, 3(08):S08003. 437 p, 2008. URL <https://cdsweb.cern.ch/record/1129811/>. Cited on pages 11 and 12.
- 1065 [19] Joao Pequenao. Computer generated image of the whole ATLAS detector,
1066 Mar 2008. URL <http://cds.cern.ch/record/1095924>. Cited on page
1067 12.
- 1068 [20] ATLAS Collaboration. Event display for one of the monojet candidates in
1069 the data. The event has a jet with $\text{pt} = 602 \text{ GeV}$ at $\eta = -1$ and $\phi =$
1070 2.6 , $\text{MET} = 523 \text{ GeV}$, and no additional jet with $\text{pt}_{\text{jet}} > 30 \text{ GeV}$ in the fi-
1071 nal state.. [https://atlas.web.cern.ch/Atlas/GROUPS/PHYSICS/](https://atlas.web.cern.ch/Atlas/GROUPS/PHYSICS/CONFNOTES/ATLAS-CONF-2011-096/fig_08.png)
1072 [CONFNOTES/ATLAS-CONF-2011-096/fig_08.png](https://atlas.web.cern.ch/Atlas/GROUPS/PHYSICS/CONFNOTES/ATLAS-CONF-2011-096/fig_08.png), 2011. Accessed:
1073 2014-03-28. Cited on page 13.
- 1074 [21] ATLAS Collaboration. Physics at a High-Luminosity LHC with ATLAS. Jul
1075

- 1079 2013. URL <https://cds.cern.ch/record/1564937>. Cited on page
1080 15.
- 1081 [22] J. Alwall, M. Herquet, F. Maltoni, O. Mattelaer, and T. Stelzer. MadGraph
1082 5: going beyond. *Journal of High Energy Physics*, 6:128, June 2011. doi:
1083 10.1007/JHEP06(2011)128. Cited on pages 15 and 33.
- 1084 [23] Torbjörn Sjöstrand, Stephen Mrenna, and Peter Skands. A brief introduc-
1085 tion to {PYTHIA} 8.1. *Computer Physics Communications*, 178(11):852 –
1086 867, 2008. ISSN 0010-4655. doi: [http://dx.doi.org/10.1016/j.cpc.2008.
1087 01.036](http://dx.doi.org/10.1016/j.cpc.2008.01.036). URL [http://www.sciencedirect.com/science/article/
1088 pii/S0010465508000441](http://www.sciencedirect.com/science/article/pii/S0010465508000441). Cited on pages 15 and 33.
- 1089 [24] The ROOT Team. Root. <http://root.cern.ch/drupal/>, 2014. Ac-
1090 cessed: 2014-03-28. Cited on page 15.
- 1091 [25] S. Agostinelli, J. Allison, K. Amako, J. Apostolakis, H. Araujo, P. Arce,
1092 M. Asai, D. Axen, S. Banerjee, G. Barrand, F. Behner, L. Bellagamba,
1093 J. Boudreau, L. Broglia, A. Brunengo, H. Burkhardt, S. Chauvie, J. Chuma,
1094 R. Chytracek, G. Cooperman, G. Cosmo, P. Degtyarenko, A. Dell'Acqua,
1095 G. Depaola, D. Dietrich, R. Enami, A. Feliciello, C. Ferguson, H. Fe-
1096 sefeldt, G. Folger, F. Foppiano, A. Forti, S. Garelli, S. Giani, R. Gi-
1097 annitrapani, D. Gibin, J.J. Gómez Cadenas, I. González, G. Gracia
1098 Abril, G. Greeniaus, W. Greiner, V. Grichine, A. Grossheim, S. Guatelli,
1099 P. Gumligner, R. Hamatsu, K. Hashimoto, H. Hasui, A. Heikkinen,
1100 A. Howard, V. Ivanchenko, A. Johnson, F.W. Jones, J. Kallenbach, N. Kanaya,
1101 M. Kawabata, Y. Kawabata, M. Kawaguti, S. Kelner, P. Kent, A. Kimura,
1102 T. Kodama, R. Kokoulin, M. Kossov, H. Kurashige, E. Lamanna, T. Lampén,
1103 V. Lara, V. Lefebure, F. Lei, M. Liendl, W. Lockman, F. Longo, S. Magni,
1104 M. Maire, E. Medernach, K. Minamimoto, P. Mora de Freitas, Y. Morita,
1105 K. Murakami, M. Nagamatu, R. Nartallo, P. Nieminen, T. Nishimura, K. Oht-
1106 subo, M. Okamura, S. O'Neale, Y. Oohata, K. Paech, J. Perl, A. Pfeiffer,
1107 M.G. Pia, F. Ranjard, A. Rybin, S. Sadilov, E. Di Salvo, G. Santin, T. Sasaki,
1108 N. Savvas, Y. Sawada, S. Scherer, S. Sei, V. Sirotenko, D. Smith, N. Starkov,
1109 H. Stoecker, J. Sulkimo, M. Takahata, S. Tanaka, E. Tcherniaev, E. Safai
1110 Tehrani, M. Tropeano, P. Truscott, H. Uno, L. Urban, P. Urban, M. Verderi,
1111 A. Walkden, W. Wander, H. Weber, J.P. Wellisch, T. Wenaus, D.C. Williams,
1112 D. Wright, T. Yamada, H. Yoshida, and D. Zschiesche. Geant4—a sim-
1113 ulation toolkit. *Nuclear Instruments and Methods in Physics Research*
1114 *Section A: Accelerators, Spectrometers, Detectors and Associated Equip-
1115 ment*, 506(3):250 – 303, 2003. ISSN 0168-9002. doi: [http://dx.doi.org/
1116 10.1016/S0168-9002\(03\)01368-8](http://dx.doi.org/10.1016/S0168-9002(03)01368-8). URL <http://www.sciencedirect.com/science/article/pii/S0168900203013688>. Cited on page 17.
- 1117 [26] ATLAS Collaboration. Performance assumptions for an upgraded ATLAS
1118 detector at a High-Luminosity LHC. Mar 2013. URL <https://cds.cern.ch/record/1527529/>. Cited on pages 17, 20, 26, 27, and 28.
- 1119 [27] ATLAS Collaboration. Electron performance measurements with the ATLAS
1120

1122 detector using the 2010 LHC proton-proton collision data. *Eur. Phys. J. C*,
1123 72(arXiv:1110.3174. CERN-PH-EP-2011-117):1909. 45 p, Oct 2011. Com-
1124 ments: 33 pages plus author list (45 pages total), 24 figures, 12 tables, sub-
1125 mitted to Eur. Phys. J. C. Cited on pages 26 and 28.

1126 [28] ATLAS Collaboration. Search for New Phenomena in Monojet plus Missing
1127 Transverse Momentum Final States using 10fb-1 of pp Collisions at $\sqrt{s}=8$
1128 TeV with the ATLAS detector at the LHC. Nov 2012. URL [http://cds.
1129 cern.ch/record/1493486/](http://cds.cern.ch/record/1493486/). Cited on pages 32, 33, 34, 36, 37, and 43.

1130 [29] Donald Duck. The history of automatic control. *Duckburg Journal of Sci-
1131 ence*, 106(3):345–401, 2005. Cited on page 48.

1133 **Upphovsrätt**

1134 Detta dokument hålls tillgängligt på Internet — eller dess framtida ersättare —
 1135 under 25 år från publiceringsdatum under förutsättning att inga extraordinära
 1136 omständigheter uppstår.

1137 Tillgång till dokumentet innebär tillstånd för var och en att läsa, ladda ner,
 1138 skriva ut enstaka kopior för enskilt bruk och att använda det oförändrat för icke-
 1139 kommersiell forskning och för undervisning. Överföring av upphovsrätten vid
 1140 en senare tidpunkt kan inte upphäva detta tillstånd. All annan användning av
 1141 dokumentet kräver upphovsmannens medgivande. För att garantera äktheten,
 1142 säkerheten och tillgängligheten finns det lösningar av teknisk och administrativ
 1143 art.

1144 Upphovsmannens ideella rätt innehåller rätt att bli nämnd som upphovsman
 1145 i den omfattning som god sed kräver vid användning av dokumentet på ovan
 1146 beskrivna sätt samt skydd mot att dokumentet ändras eller presenteras i sådan
 1147 form eller i sådant sammanhang som är kränkande för upphovsmannens litterära
 1148 eller konstnärliga anseende eller egenart.

1149 För ytterligare information om Linköping University Electronic Press se för-
 1150 lagets hemsida <http://www.ep.liu.se/>

1151 **Copyright**

1152 The publishers will keep this document online on the Internet — or its possi-
 1153 ble replacement — for a period of 25 years from the date of publication barring
 1154 exceptional circumstances.

1155 The online availability of the document implies a permanent permission for
 1156 anyone to read, to download, to print out single copies for his/her own use and
 1157 to use it unchanged for any non-commercial research and educational purpose.
 1158 Subsequent transfers of copyright cannot revoke this permission. All other uses
 1159 of the document are conditional on the consent of the copyright owner. The
 1160 publisher has taken technical and administrative measures to assure authenticity,
 1161 security and accessibility.

1162 According to intellectual property law the author has the right to be men-
 1163 tioned when his/her work is accessed as described above and to be protected
 1164 against infringement.

1165 For additional information about the Linköping University Electronic Press
 1166 and its procedures for publication and for assurance of document integrity, please
 1167 refer to its www home page: <http://www.ep.liu.se/>